

FASCODE For The Environment

**H.E. Snell
W.O. Gallery
J.-L. Moncet
C.P. Sarkisian**

**Atmospheric and Environmental Research, Inc.
840 Memorial Drive
Cambridge, MA 02139-3794**

20 Nov 2000

Scientific Report No. 3

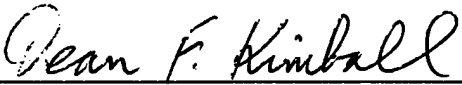
APPROVED FOR PUBLIC RELEASE; DISTRIBUTION UNLIMITED.


20020524 115



**AIR FORCE RESEARCH LABORATORY
Space Vehicles Directorate
29 Randolph Rd
AIR FORCE MATERIEL COMMAND
Hanscom AFB, MA 01731-3010**

This technical report has been reviewed and is approved for publication.


DEAN F. KIMBALL
Contract Manager


DUANE E. PAULSEN
Deputy Chief, AFRL/VSSS

This report has been reviewed by the ESC Public Affairs Office (PA) and is releasable to the National Technical Information Service (NTIS).

Qualified requestors may obtain additional copies from the Defense Technical Information Center (DTIC). All others should apply to the National Technical Information Service (NTIS).

If your address has changed, if you wish to be removed from the mailing list, or if the addressee is no longer employed by your organization, please notify PL/IM, 29 Randolph Road, Hanscom AFB MA 01731-3010. This will assist us in maintaining a current mailing list.

Do not return copies of this report unless contractual obligations or notices on a specific document require that it be returned.

REPORT DOCUMENTATION PAGEForm Approved
OMB No. 0704-0188

Public reporting burden for this collection of information is estimated to average 1 hour per response, including the time for reviewing instructions, searching existing data sources, gathering and maintaining the data needed, and completing and reviewing the collection of information. Send comments regarding this burden estimate or any other aspect of this collection of information, including suggestions for reducing the burden, to Washington Headquarters Services, Directorate for Information Operations and Reports, 1215 Jefferson Davis Highway, Suite 1204, Arlington, VA 22202-4302, and to the Office of Management and Budget, Paperwork Reduction Project (0704-0188), Washington, DC 20503.

1. AGENCY USE ONLY (Leave blank)	2. REPORT DATE January 15, 2000	3. REPORT TYPE AND DATES COVERED Scientific Report #3, 10 June 1997 - 28 February 1999
----------------------------------	------------------------------------	---

4. TITLE AND SUBTITLE FASCODE for the Environment (FASE)	5. FUNDING NUMBERS Contract F19628-93-C-0040 PE 63215C
---	--

6. AUTHOR(S) H.E. Snell, W.O. Gallery, J.-L. Moncet and C.P. Sarkisian	PR5321 TAGD WUAD
---	------------------------

7. PERFORMING ORGANIZATION NAMES(S) AND ADDRESS(ES) Atmospheric and Environmental Research, Inc. 131 Hartwell Avenue Lexington, MA 02412	8. PERFORMING ORGANIZATION REPORT NUMBERS Project No. P-519
---	--

9. SPONSORING / MONITORING AGENCY NAMES(S) AND ADDRESS(ES) Air Force Research Laboratory 29 Randolph Road Hanscom AFB, MA 01731-3010	10. SPONSORING / MONITORING AGENCY REPORT NUMBER AFRL-VS-TR-2001-1603
---	---

11. SUPPLEMENTARY NOTES Contract Manager: Dean Kimball

12a. DISTRIBUTION/AVAILABILITY STATEMENT Approved for public release; distribution unlimited	12b. DISTRIBUTION CODE
---	------------------------

13 ABSTRACT (Maximum 200 words)
FASCODE for the Environment (FASE) is the latest in a long line of atmospheric transmittance and radiance models developed by the Battlespace Environment Division of the Air Force Research Laboratory (AFRL), formerly known as the Optical Physics Division of the Geophysics Directorate, USAF Phillips Laboratory, and before that, the Air Force Geophysics Laboratory (AFGL). FASE is a direct descendent of the line-by-line atmospheric transmittance/radiance model FASCOD3. It also incorporates recent developments from the similar model LBLRTM. This report presents the additions and improvements in FASE over previous models, including: 1. improvements and corrections to the geometry routines, 2. corrections to the NLTE routines, 3. corrections to the blackbody function when aerosols are included, 4. corrections and improvements to the Hartley-Huggins and the Hertzberg continua, 5. corrections to the calculations of absorption cross-sections and to the laser calculation, 6. addition of the Schumann-Runge Band and continuum, 7. inclusion of a solar spectrum module, 8. inclusion of a spectral limit check when line coupling is included, and 9. acceptance of the HITRAN96 line parameters.

14. SUBJECT TERMS FASE, FASCODE, HITRAN, LBLRTM, Raditive transfer, Line-by-line, Infrared radiance, Atmospheric radiance	15. NUMBER OF PAGES 76
	16. PRICE CODE

17. SECURITY CLASSIFICATION OF REPORT Unclassified	18. SECURITY CLASSIFICATION OF THIS PAGE Unclassified	19. SECURITY CLASSIFICATION OF ABSTRACT Unclassified	20. LIMITATION OF ABSTRACT SAR
--	---	--	-----------------------------------

TABLE OF CONTENTS

1. Introduction	1
2. Model Comparisons	2
2.1. Features Comparison	2
2.1.1. Voigt Function Algorithm	3
2.1.2. Vectorization	11
2.1.3. Parameterization	11
2.1.4. Line Rejection Flag	11
2.1.5. Multiple Scattering	12
2.1.6. LASER Capability	12
2.1.7. Non-LTE Option	12
2.1.8. Scanning Function	12
2.1.9. Plotting Function	13
2.1.10. Aerosol/Cloud Attenuation	13
2.1.11. Spectral Limit	13
2.1.12. INPUT/OUTPUT Routes	13
2.1.13. Geometry Package	13
2.2. Numerical Comparison	14
2.3. Conclusions	20
3. Upgrades to Existing Features	21
3.1. Geometry Routines	21
3.1.1. Input/Output Module	21
3.1.2. Identification of Existing Deficiencies	22
3.1.3. Resolution of Deficiencies	22
3.1.4. Validation of Geometry module	25
3.2. Chappuis And Wulf Ozone Bands	28
3.3. Non-Local Thermodynamic Equilibrium (NLTE)	29
3.4. Black-Body Approximation	29
3.5. Emissivity/Reflectivity	29
3.5.1. Input File Format	30
3.6. Hartley-Huggins Continuum / Herzberg Continuum	30
3.7. Absorption Cross-Sections	31
3.8. Layer Input/Output Units	31
3.9. Laser Calculations	31
4. New Features	32
4.1. Schumann-Runge Band and Continuum	32

4.2. Solar Spectrum	33
4.2.1. File Structure	34
4.2.2. Implementation.....	34
4.2.3. Calculations with the Solar Irradiance Option	35
4.3. Line Coupling.....	36
4.4. HITRAN96 Line Parameters	37
4.5. HITRAN96 Heavy-Molecule Cross-Sections	37
4.5.1. Accuracy of Pseudo-Line Approach.....	38
4.5.2. Pseudo-Line Timing Tests.....	50
4.5.3. Pseudo-Line Algorithm Implementation	51
4.5.4. Execution of FASE with Pseudo-Lines.....	53
4.6. Cloud/Rain Upgrades	54
5. Suggestions for Future Upgrades and Model Validation	56
5.1. Multiple Scattering	56
5.2. Cloud/Rain Upgrades	56
5.3. Beta-Test Results.....	56
5.4. Calibration and Validation	57
6. Summary	58
7. References	59
Appendix A: Spectral Grid Algorithm.....	63

LIST OF FIGURES

Figure 1 FASE(201) and FASCODE Differences	9
Figure 2 FASE(201) and FASE(2001) Differences	10
Figure 3 FASE(2001) and FASCODE Differences	10
Figure 4 Comparison of FASCODE and LBLRTM Transmission for CASE1: p=972.2107, T=285.9446	17
Figure 5 Comparison of FASCODE and LBLRTM Transmission for CASE2: p=130.4209, T=216.7	18
Figure 6 Comparison of FASCODE and LBLRTM Transmission for CASE3: p=0.1251, T=235.9188	19
Figure 7 Absorption Cross-Section from the FASE Calculation for a 1km Path at p=169.9 torr, T=216.0 K (path amount of F-12=1.814E+14 molecules cm ⁻²).....	39
Figure 8 Absorption Cross-Section as Computed from the FASE Calculation for a 1km Path at p=700.3 torr, T=296.2 K (path amount of F-12=5.437E+14 molecules cm ⁻²).....	40
Figure 9 Percent Difference Between the Cross-Section Computed with Pseudo-Lines and the Data from Varanasi for a 1km Path at p=169.9 torr, T=216.0 K.....	40
Figure 10 Percent Difference Between the Cross-Section Computed with Pseudo-Lines and the Data from Varanasi for a 50km Path at p=169.9 torr, T=216.0 K.....	41
Figure 11 Percent Difference Between the Cross-Section Computed with Pseudo-Lines and the Data from Varanasi for a 1km Path at p=700.3 torr, T=296.2 K.....	41
Figure 12 Percent Difference Between the Cross-Section Computed with Pseudo-Lines and the Data from Varanasi for a 50km Path at p=700.3 torr, T=296.2 K.....	42
Figure 13 Difference Between Computed and Measured Cross-Section for a 1km Path at p=169.9 torr, T=216.0 K	42
Figure 14 Comparison of the Computed Cross-Section (Solid Line) with the Measured Cross-Section (Dotted) for the Conditions Given in Figure 7 Over the Range 860- 880 cm ⁻¹	43
Figure 15 Comparison of the Computed Cross-Section (Solid Line) with the Measured Cross-Section (Dotted) for the Conditions Given in Figure 7 Over the Range 880- 900 cm ⁻¹	43
Figure 16 Comparison of the Computed Cross-Section (Solid Line) with the Measured Cross-Section (Dotted) for the Conditions Given in Figure 7 Over the Range 900- 910 cm ⁻¹	44

Figure 17 Comparison of the Computed Cross-Section (Solid Line) with the Measured Cross-Section (Dotted) for the Conditions Given in Figure 7 Over the Range 920-925 cm^{-1}	44
Figure 18 Comparison of the Computed Cross-Section (Solid Line) with the Measured Cross-Section (Dotted) for the Conditions Given in Figure 7 Over the Range 942-944 cm^{-1}	45
Figure 19 Comparison of the Computed Cross-Section (Solid Line) with the Measured Cross-Section (Dotted) for the Conditions Given in Figure 8 Over the Range 860-880 cm^{-1}	45
Figure 20 Comparison of the Computed Cross-Section (Solid Line) with the Measured Cross-Section (Dotted) for the Conditions Given in Figure 8 Over the Range 880-900 cm^{-1}	46
Figure 21 Comparison of the Computed Cross-Section (Solid Line) with the Measured Cross-Section (Dotted) for the Conditions Given in Figure 8 Over the Range 900-910 cm^{-1}	46
Figure 22 Comparison of the Computed Cross-Section (Solid Line) with the Measured Cross-Section (Dotted Line) for the Conditions Given in Figure 8 Over the Range 920-925 cm^{-1}	47
Figure 23 Comparison of the Computed Cross-Section (Solid Line) with the Measured Cross-Section (Dotted) for the Conditions Given in Figure 8 Over the Range 942-944 cm^{-1}	47
Figure 24 Measurements of F-12 in the Far Wings of the Band	48
Figure 25 Example of the New FASE Cloud Options: User has the Ability to Change Cloud Base Altitude and Thickness	55

LIST OF TABLES

Table 1 Model Comparisons	3
Table 2 Percent Difference in Layer Convolution Time Between Model Configurations.....	7
Table 3 Total Model Run Time Comparisons.....	7
Table 4 Evaluation of Time Saved.....	8
Table 5 Parameters for FASCODE/LBLRTM Comparisons.....	16
Table 6 TAPE5 Input Parameters.....	21
Table 7 ITYPE=2 Input Parameters.....	22
Table 8 New and Modified Routines	24
Table 9 Case 2A Model Comparisons for Geometry	25
Table 10 Case 2B Model Comparisons for Geometry (N,O = new,old FASE, M = MODTRAN; for PHI = 90° MODTRAN2 is unable to find the tangent point)	26
Table 11 Case 2C/2D Model Comparisons for Geometry (H1=H2=5km)	27
Table 12 Case 2C Geometry Test Results.....	28
Table 13 Values Computed to Define Path Geometry	28
Table 14 Values Used in Propagation of Error Calculations	50
Table 15 Timing Test Results	51
Table 16 Fundamental Vibrational Frequencies for F-12	53
Table 17 Molecules Without Profiles.....	54
 Table A- 1 Model Comparisons for Total CPU Run Time	 64
Table A- 2 Case1: Limb Calculation with 12km Tangent Height	64
Table A- 3 Case 2: Looking Up: 0km - 100km.....	65
Table A- 4 Case 3: Looking Down: 100km - 0km.....	66

1. Introduction

FASCODE for the Environment (FASE) is the latest in a long line of atmospheric transmittance and radiance models developed by the Optical Physics Division of the Geophysics Directorate, USAF Phillips Lab (Anderson et al., 1995). Of interest to this project is the high spectral resolution Fast Atmospheric Signature Code, "FASCODE" (Smith et al., 1978). The most recent version, FASCOD3P, was released circa 1992. Line-by-line models such as FASCODE calculate atmospheric molecular transmittance from first principles, the core of which is a fast algorithm to calculate the Voigt line shape. The Voigt algorithm, coupled with the best available physics and latest atmospheric models and data, makes FASCODE an accurate and efficient model for atmospheric transmittance and radiance. Further, it is accepted as a reference standard model for the scientific community.

After the FASCOD3P release, work on the model continued at AER in two different directions. Internally, AER modified FASCOD3P for application to inversion problems and sensor studies (this code is called XFWD and is described in Miller et al., 1995). The Department of Energy (DOE) Atmospheric Radiation Measurement Program (DOE-ARM) also sponsored AER for the development of the Line-By-Line Radiative Transfer Model (LBLRTM), with the main goal of further improving the physics through the analysis of atmospheric measurements made at various ARM experimental sites (Clough et al., 1993). LBLRTM is derived from FASCOD3P and includes a number of significant advancements and changes.

Both XFWD and LBLRTM are significantly different in capabilities from FASCOD3P. In particular, certain capabilities of FASCOD3P (multiple scattering, non-LTE emission, and aerosol attenuation) were removed for these specialized applications. The FASE model was developed to continue the FASCODE-series of models while meeting the following criteria:

- incorporate the best features and advancements from LBLRTM and other models,
- preserve all the capabilities of FASCOD3P,
- improve the user interface, and
- add other features and improvements as resources permit.

This report describes the work performed in developing FASE and addresses upgrades to existing FASCOD3P features, the addition of new features, numerical, algorithm and coding comparisons among the various models, and suggestions for future code development.

2. Model Comparisons

In choosing the starting point from which to develop FASE we compared three line-by-line radiative transfer codes: FASCOD3P (Phillips Laboratory), a modified version of FASCOD3 (an internal product of AER not intended for public release), and the "global release", September 1994, version of LBLRTM (AER / ARM). It should be noted that all three models are similar in that they were derived from earlier versions of FASCOD; the modified version of FASCOD3 can be considered an intermediate step between FASCOD3 and LBLRTM. The object of this internal study was to determine which of the three models (FASCOD3P, the modified version of FASCOD3, or LBLRTM) would allow us to spend a minimal amount of time re-coding features from other models so that our time could be spent updating, and adding to, the model physics. This model comparison was accomplished through a side-by-side examination of the three models. In addition we also investigated the cause of observed differences in the radiances calculated with FASCOD3P and with LBLRTM, including both timing and numerical comparisons. The following sections report the results of these comparisons.

Section 2.1 describes the differences in algorithm features and, where applicable, their impact on the accuracy of the calculation; Section 2.2 describes numerical differences between the codes for a set of test cases.

2.1. Features Comparison

Table 1 is a partial list of the distinguishing characteristics of the three models. It provides a comparison of FASCOD3P, the AER-modified version of FASCOD3, and a "global release" version of LBLRTM. It should be noted that while this is only a partial list of the differences, it represents features important to the development of FASE.

Table 1 Model Comparisons

Features	Model		
	FASCODE3P	Modified FASCOD3	LBLRTM
Voigt Function	Old	Old	New
Vectorized	No	No	Yes
Parameterized	None	Some	Extensive
Line Rejection Flag	No	No	Yes
Multiple Scattering	Internal	None	Output in correct format for external codes (e.g., CHARTS or DISORT)
LASER Option	Yes	No	No
Non-LTE Option	Yes	No	No
Scanning Function	SCANFN	SCANFN	FFTSCAN and SCANFN
Plotting Function	FASPLT	FASPLT	LBLPLT with NCAR Graphics Option
Aerosol/Cloud Attenuation	Yes	No	Yes
Spectral Bandwidth Limit	520 cm ⁻¹	520 cm ⁻¹	2020 cm ⁻¹
I/O Routines (BUFIN/BUFOUT) Function	Old	New	New
Geometry Package	FSCATM	FSCATM	LBLATM

2.1.1. Voigt Function Algorithm

Atmospheric infrared absorption lines are described by the Voigt line shape, which is the convolution of the Lorentz and Doppler line shapes. The Voigt function has no analytic expression and considerable effort by many authors has been devoted to finding efficient and accurate approximations. At the core of the FASCODE model is a very fast Voigt algorithm that calculates the Voigt function via a lineshape decomposition (Clough and Kneizys, 1979). However, recent advances in the accuracy of field measurements and the corresponding more stringent requirements for simulations require even greater accuracy for the Voigt function. LBLRTM has modified the Voigt function from FASCODE to increase the accuracy. This work is one of the driving factors behind FASE as it could significantly impact the calculations under certain scenarios, particularly atmospheric parameter retrieval problems.

The FASCODE lineshape algorithm decomposes the Voigt lineshape function into a summation of functions representing the Lorentz and Doppler components as well as an error term to account for small differences from these functional approximations:

$$\begin{aligned}
 V(\xi, z) = & C_1(\xi)F_1(z) + C_2(\xi)F_2(z) + C_3(\xi)F_3(z) \\
 & + \frac{\alpha_c}{\alpha_v}[F_4(z) + F_5(z)] + C_D(\xi)F_D(z) \\
 & + C_{v_\epsilon}(\xi)V_\epsilon(z)
 \end{aligned}
 \tag{Eq. 1}$$

where

$$\xi = \frac{\alpha_c}{\alpha_c + \alpha_D}
 \tag{Eq. 2}$$

and

$$z = \frac{v - v_i}{\alpha_v}
 \tag{Eq. 3}$$

In these equations:

- v = frequency in wavenumbers
- v_i = frequency of the i 'th spectral transition
- α_v, α_c , and α_D = the Voigt, Lorentz and Doppler halfwidths
- $C_i, i = 1, 2, 3, D, \epsilon$ = coefficients
- $F_i, i = 1, 2, \dots, 5, D$ = shape functions
- V_ϵ = error shape function

The Lorentz component is described by the first four functions in the Doppler with a single function (subscript D), and the error with the remaining term. The coefficients, $C(\xi)$, are tabulated in data statements within the code, and the shape functions, $F(z)$, are computed within the code.

In both FASCODE and FASE there are 102 coefficients stored in data statements. However, to determine the coefficient corresponding to the value of ξ , FASE linearly interpolates between coefficients while FASCODE merely chooses the coefficient closest to the calculated value of ξ . The shape functions are also computed in a slightly different manner: FASE computes $F(z)$ on a grid of 2001 points while FASCODE computes only 201 points. The combination of these two

changes in FASE decreased the errors associated with the lineshape computation as compared to measurements (Clough and Brown, 1994), but increased the overall computation time. In FASE this timing penalty was offset through the optimization of other parts of the algorithm coding, namely the BUFIN/BUFOUT routines. This study evaluates the differences between the original FASCODE method and the FASE improvements in order to:

- determine whether or not the changes are justified in terms of accuracy / timing considerations, and
- decide whether there is a less computationally expensive way to achieve the numerical accuracy of the increased points and interpolation.

One should note that the number of points and interpolation differences appear in the convolution routine for the first three functions, while the so-called fourth-function is different because it only interpolates the halfwidth ratio (the same number of points are used to define the lineshape function). Because the interpolation time for the fourth-function is very small compared to the other functions, comparison of fourth-function timing gives a measure of the numerical stability of the timing test.

2.1.1.1. Voigt Function Timing Tests

The comparison of model timing can be difficult since the time will vary depending on machine load and network traffic. To minimize this effect, 30 runs of the models were compared. Further, the runs were done after midnight on a (nearly) dedicated machine to reduce the competition for CPU and disk access time. A total of three different model configurations were used to ascertain timing differences: FASE, FASCODE, and FASE with only 201 points for the shape functions, hereafter denoted as FASE2001, FASCD3P, and FASE201. Because of coding differences such as BUFIN/BUFOUT (the file I/O routines), the layer convolution times, rather than the total run time, were the basis for the comparison (a multiple-layer profile was used in order to increase the number of points for comparison). Comparison of FASE2001 with FASCD3P will show the overall change in CPU time, comparison of FASE2001 with FASE201 will illustrate the additional time due to the increased number of points, and comparison of FASCD3P with FASE201 will show the effect of the coefficient interpolation. To minimize differences in the overall timing of the codes, only the optical depth was computed.

Three types of tests were used to compare the convolution times:

1. 20 layer atmosphere from 0 to 25 km (looking up),
2. 22 layer path from 100 km, through a tangent at 25 km, to space, and
3. 22 layer path from 50 km, through a tangent at 5 km, and back up to 50 km.

All tests were over the spectral interval from 2050 - 2075 cm^{-1} ; subtle differences between FASE and FASCODE were eliminated by explicitly specifying the atmospheric layering and by setting ALFALO to 0.04 cm^{-1} . The tangent path of Case 2 was tested twice, once after midnight on a Sunday morning, to judge the effect of computer load on the timing. The results of these tests are given in Table 2 through Table 4, summarizing the layer convolution times, total model run times, and total time savings.

The percent difference in layer convolution times between the model configurations were computed for each layer and averaged over all of the runs. "Mean" refers to the mean ratio over all the layers and all of the test runs, "RMS" is the root-mean-square variation from this mean, and "Savings" is the percent time saved, equal to $(1 - \text{Mean})$. The ratio of FASCD to FASE2001 shows the effect of increasing the number of points used to describe the line shape and interpolating between the coefficients, FASCD / FASE201 shows the effect of the interpolation, and FASE201 / FASE2001 shows the effect of the increased number of points. The "savings" given in the first row of each case should be the sum of the next two rows, but this is not exactly true because of differences between other portions of the FASE and FASCODE algorithms. The ratio of FASE runs for LBLF4 gives an indication of the stability of the test since this subroutine is the same for both of the FASE models.

For the up-looking case (Case 1) and for the lower-altitude limb case (Case 3), eliminating the interpolation saves more time than decreasing the number of points. The opposite is true for the high-altitude limb tests (Case 2). This illustrates that determining the effect of changes to the model involves a complex relation between the algorithm itself and the characteristics of the atmospheric path. One should also note that in the high-altitude tangent cases the time saved by model changes is much less than for the other test cases. This could be due to the higher spectral dv required for this case. In any event, this illustrates the difficulty of evaluating, for all scenarios, the timing impact of model changes.

Table 2 Percent Difference in Layer Convolution Time Between Model Configurations

Case	Ratio	HIRAC			LBLF4		
		Mean	Savings	RMS	Mean	Savings	RMS
1	FASCD/FASE2001	81.69%	18.31%	5.37%	105.71%	-5.71%	17.74%
	FASCD/FASE201	86.35%	13.65%	5.67%	105.74%	-5.74%	17.68%
	FASE 201/2001	94.61%	5.39%	1.45%	99.98%	0.02%	1.81%
2A	FASCD/FASE2001	94.36%	5.64%	2.09%	98.44%	1.56%	3.87%
	FASCD/FASE201	99.51%	0.49%	1.63%	98.23%	1.77%	3.50%
	FASE 201/2001	94.83%	5.17%	1.66%	100.21%	-0.21%	1.31%
2B	FASCD/FASE2001	94.15%	5.85%	0.86%	98.29%	1.71%	3.35%
	FASCD/FASE201	99.40%	0.60%	0.86%	98.20%	1.80%	3.32%
	FASE 201/2001	94.72%	5.28%	0.30%	100.09%	-0.09%	0.09%
3	FASCD/FASE2001	87.75%	12.25%	5.86%	102.25%	-2.25%	8.97%
	FASCD/FASE201	92.98%	7.02%	5.70%	102.62%	-2.62%	8.87%
	FASE 201/2001	94.37%	5.63%	2.41%	99.65%	0.35%	2.38%

Table 3 Total Model Run Time Comparisons

Case	Model	Mean (seconds)	RMS
1	FASE 2001	111.33	8.40
	FASE 201	109.12	11.13
	FASCODE	154.57	19.30
2A	FASE 2001	297.13	15.85
	FASE 201	292.57	19.98
	FASCODE	389.81	29.29
2B	FASE 2001	287.77	1.17
	FASE 201	286.31	0.91
	FASCODE	378.02	18.11
3	FASE 2001	199.59	15.98
	FASE 201	195.80	14.40
	FASCODE	270.58	21.01

Table 4 Evaluation of Time Saved

		Case 1	Case 2A	Case 2B	Case 3
HIRAC	Savings without interpolation	4.51%	0.03%	0.04%	1.10%
	Savings without increased points	1.78%	0.30%	0.31%	0.88%
	Total Savings	6.04%	0.33%	0.35%	1.92%
	Time Saved	6.72 sec	0.98 sec	1.01 sec	3.83 sec
TOTAL	Savings without interpolation	3.55%	1.18%	1.24%	-0.21%
	Savings without increased points	6.05%	0.16%	0.25%	1.06%
	Total Savings	5.09%	1.34%	1.50%	0.80%
	Time Saved	5.67 sec	3.98 sec	4.32 sec	1.60 sec

A comparison of total model run times, expressed in seconds, is given in Table 3. The mean value is over the 30 runs tested for each case. Case 2B was run after midnight on a Sunday morning and the RMS variations in the total times are much less than for the other cases. Note that the total run times are not indicative of the timing differences between the models because of other differences in the algorithm coding. Case 2 was significantly longer than the other cases because the higher altitudes require calculations on a smaller spectral grid.

Given the relative changes in the individual convolution routines and the total time to run each model, it is straightforward to calculate the amount of time that will be saved by making the changes. However, the models have slightly different coding for many of the routines, due in part to the vectorization of FASE and changes to the input and output routines. Because of this, one cannot simply use the ratio of total run times to calculate differences. Thus the ratios given in Table 2 must be combined with the total times given in Table 3. The amount of time saved is given by:

$$S = \frac{\delta H}{T} + \frac{\sigma L}{T} \quad \text{Eq. 4}$$

where δ and σ are given as "Savings" in Table 2, H and L are the total time spent in the HIRAC and LBLF4 convolution routines, and T is the total model time (FASE 2001) from Table 3.

An evaluation of the amount of time saved by eliminating the interpolation of the coefficients (FASE 201 vs. FASCODE), by using fewer points to define the shape function (FASE 2001 vs. FASE 201), and by both changes (FASE 2001 vs. FASCODE) is shown in Table 4. The total savings should be the sum of the other two rows, except for differences between FASCODE and FASE auxiliary routines (e.g. BUFIN, BUFOUT, code vectorization, etc.). The time saved is relative to the FASE 2001 times given in Table 3. The "total" values for S in Table 4 are

somewhat misleading due to the negative values for the time "saved" in LBLF4. This is more of a numeric artifact than anything else since the individual layer times for LBLF4 are either very small or very large, but are always very similar. (The effect of the interpolation is very small relative to the total time; the number of points to describe the lineshape is irrelevant in this function). While Table 2 showed relatively large savings in the HIRAC convolution by using fewer points or by eliminating the interpolation, the overall effect on the model is quite small. This is true particularly in Case 2 where the convolution routines are a much smaller percentage of the total execution time than for the other cases (~6% for Case 2 vs. 15-30% for Case 1 and Case 3).

2.1.1.2. Voigt Function Numerical Differences

A single-layer case (from 22 - 25 km) was used to examine the effects of additional points to define the lineshape function and the coefficient interpolation. The results of this test, over a narrow portion of the entire spectral region, are shown in Figure 1, Figure 2, and Figure 3. Figure 1 shows the effect of interpolating the coefficients, and is relatively smooth compared to the effect of increasing the number of points used to describe the lineshape function (Figure 2). The result of both of these changes is shown in Figure 3, where the overall effect produces differences of the order of $\pm 0.5\%$.

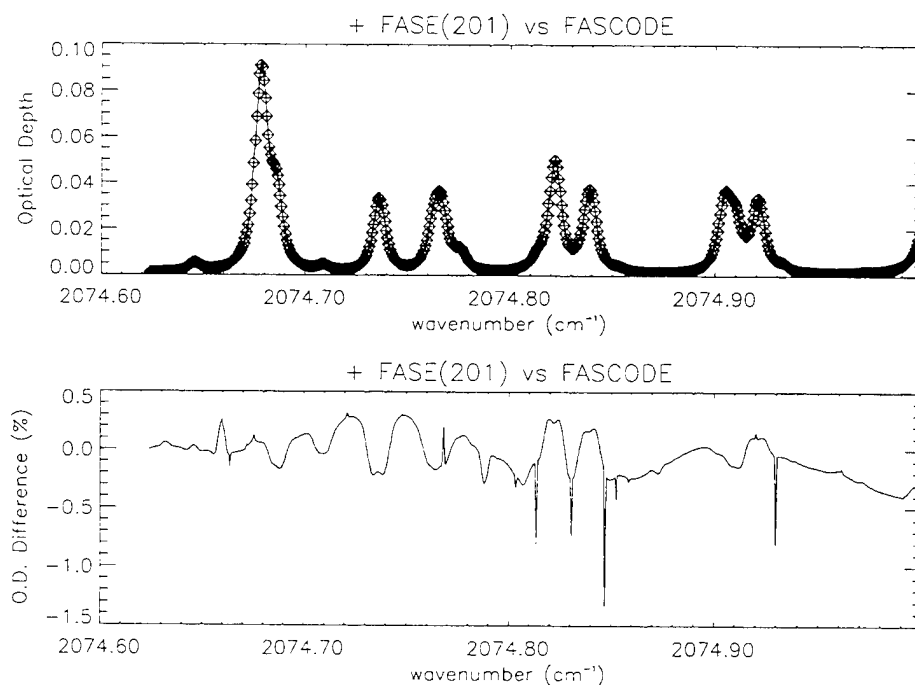


Figure 1 FASE(201) and FASCODE Differences

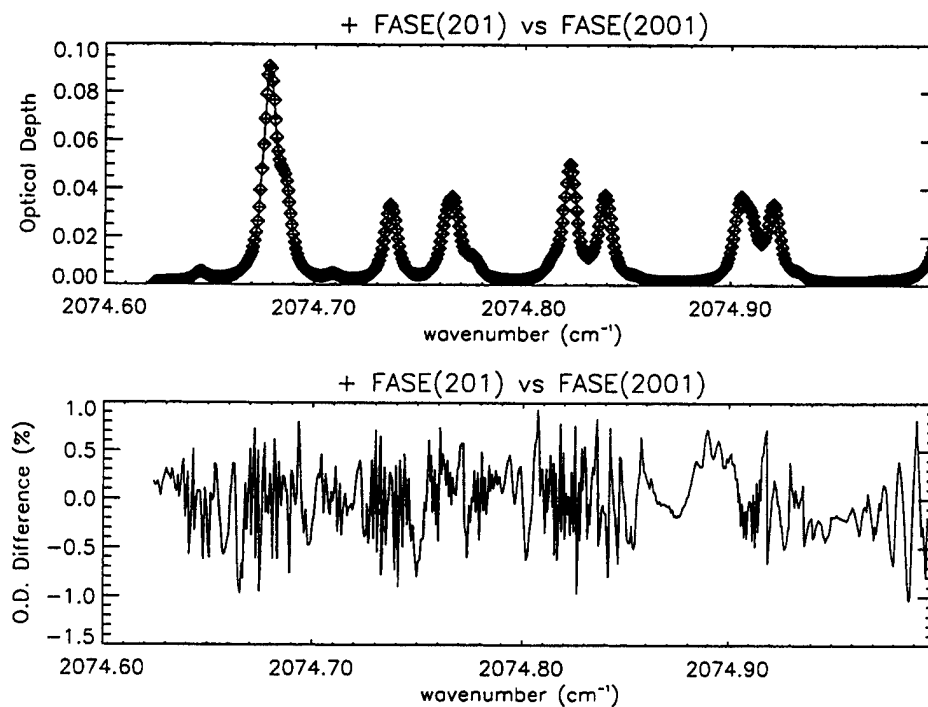


Figure 2 FASE(201) and FASE(2001) Differences

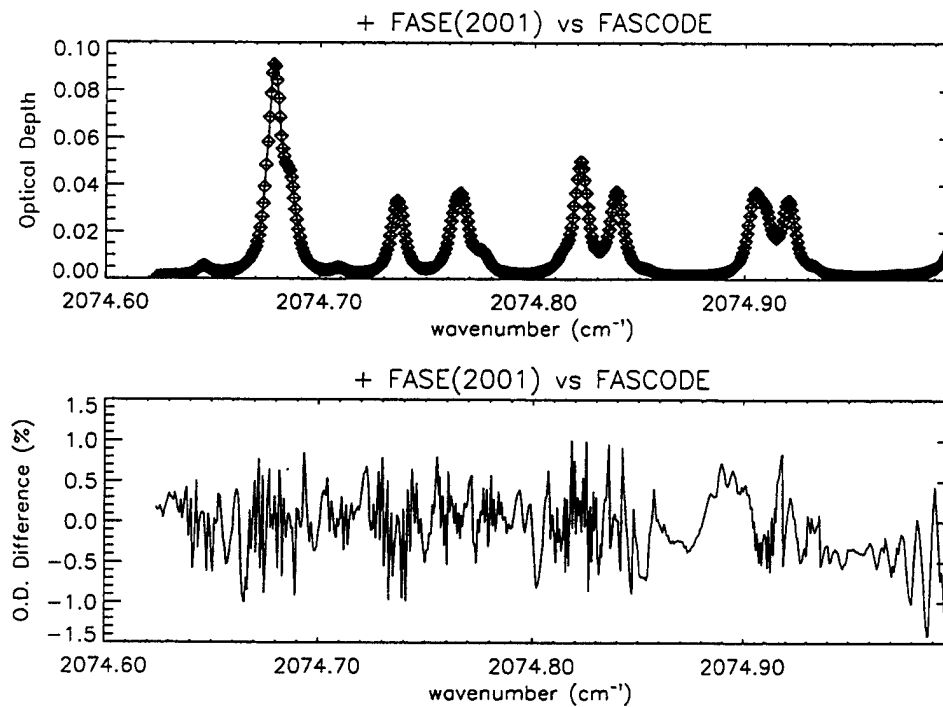


Figure 3 FASE(2001) and FASCODE Differences

It is clear from the above discussions that only a minimal amount of time can be saved by reverting to the FASCODE lineshape formulation. Further, while the optical depth differences between the "new" FASE algorithm and FASCODE are of the order of $\pm 0.5\%$, the increased accuracy is required for many remote-sensing problems. Thus the new algorithm does not increase the execution time sufficiently to warrant changes in this algorithm.

2.1.2. Vectorization

In the conversion of FASCODE to LBLRTM, many of the "do-loops" were restructured to eliminate "if-tests" from within the loops. This allows the FORTRAN compiler on vector machines to make optimal use of the machine architecture, thereby decreasing the computation time. A side benefit is that the code itself tends to be easier to read, modify, and debug.

2.1.3. Parameterization

In LBLRTM, a number of commonly used arrays were converted from "hard-wired" dimensions to dimensions that reside in parameter statements. Since these parameters were given the same names in different modules, it is relatively easy and straightforward to change the size of array dimensions. A common use of the parameterization is to increase or decrease the number of atmospheric layers that can be entered, depending on the size of the input profile (e.g. radiosonde data can contain upwards of 2000 points) and the computer memory.

2.1.4. Line Rejection Flag

Line rejection refers to the technique of rejecting a molecular absorption line from the calculation if its strength is less than a given threshold. Line rejection is determined separately for each layer and can substantially cut the computation time by eliminating a large number of weak lines whose effect on the optical depth is insignificant. The line strength threshold is determined by the requirement that the optical depth at the line center be less than some minimum value (the default is 0.0002.)

A line rejection flag was added to LBLRTM to signal whether or not a particular spectral line was rejected for use in a layer. This binary flag is stored in a file, which can be read in subsequent runs of the model so that the second run rejects the same lines as the first. This feature is particularly useful when computing radiance derivatives with respect to temperature using a finite-difference scheme since a line could be rejected in the reference case and not in the test case after perturbing the temperature or vice versa. In such cases large errors would be introduced unless the line was consistently rejected.

2.1.5. Multiple Scattering

A 2-stream approximation for multiple scattering was developed for FASCODE (Isaacs et al., 1987). This option was removed from LBLRTM in favor of an option to create the files necessary for input to a dedicated multiple scattering code, such as DISORT or CHARTS. The rationale was that many applications require more accuracy than that provided with the 2-stream approximation, and that a stand-alone, dedicated multiple scattering code is able to provide state-of-the-art accuracy with minimized computation time.

2.1.6. LASER Capability

The use of this option is important for laser calculations because of the FASCODE 4-function line decomposition algorithm (see discussion of spectral grid algorithm in Appendix A). In particular, it is possible that a specific frequency point will not be computed at all altitudes, but will instead be determined from the interpolation of adjacent spectral points. The LASER option is set up such that the optical depth at the specific LASER frequency is computed for all atmospheric layers, thus increasing the accuracy of the calculation for this specific point. This option was dropped in LBLRTM.

2.1.7. Non-LTE Option

Certain molecular species can exhibit non-equilibrium population distributions among vibrational states due to various aspects of photochemistry and reduced collision rates. This condition is known as non-local thermodynamic equilibrium, or NLTE, and mainly occurs at altitudes above 40 km. Molecules that are 'in NLTE' will exhibit thermal radiative emission that can not be described by the Planck function. A routine for NLTE that parallels the LTE optical depth routine was developed for FASCODE (Ridgway et al., 1982), but was dropped from LBLRTM.

2.1.8. Scanning Function

Many applications require that the monochromatic output of the line-by-line calculation be convolved (smoothed) with an instrument scanning function. FASCODE performs this operation with the SCANFN subroutine, which does the convolution in the frequency domain. A more efficient and accurate method is to use Fourier transform. Let S be the monochromatic spectrum, R be the instrument scanning function and let the symbols F and \star represent the Fourier transform and convolution, respectively. A fundamental theorem of Fourier transforms states that:

$$S \star R = F^{-1}(F(S) \cdot F(R)) \quad \text{Eq. 5}$$

Therefore, the convolution can be performed as the Fourier transform of the product of the transforms of the spectrum and the instrument function.

This approach has been implemented in the subroutine FFTSCAN (Gallery and Clough, 1992) which has previously been available only as a stand-alone program. In addition to being more accurate and faster than SCANFN, FFTSCAN provides for a variety of additional scanning functions.

2.1.9. Plotting Function

The plotting function was originally designed for creating graphs of the FASCODE output. Given the proliferation of specialized software for these purposes, the main utility of the plotting function is to create a 2-column ASCII output file.

2.1.10. Aerosol/Cloud Attenuation

The cloud and aerosol routines found in FASCODE and LBLRTM are derived from the routines found in LOWTRAN (Anderson et al., 1995). Recent improvements to these routines for MODTRAN (Acharya et al., 1993) allow for multiple cloud layers and an improved interface for user-supplied information (spectral properties and vertical profiles). The upgraded routines are discussed below.

2.1.11. Spectral Limit

The calculation spectral limit was changed from 520 cm^{-1} in FASCODE to 1010 cm^{-1} in LBLRTM. The larger limit is particularly useful in the mid-IR where instruments typically have a large spectral range.

2.1.12. INPUT/OUTPUT Routes

The BUFIN/BUFOUT subroutines control the unformatted input and output. The coding was changed from LBLRTM to increase the speed of the I/O.

2.1.13. Geometry Package

All three codes listed in Table 2-1 use the same geometry package (Gallery et al., 1983) which includes the calculation of refractive path. This package was found to have some numerical instabilities, particularly in short paths that are nearly tangent to the atmosphere. These errors were reduced in FASE (see Section 3.1).

2.2. Numerical Comparison

A comparison of FASCODE and LBLRTM was performed by AER and by Dr. Jinxue Wang of the Phillips Laboratory to ascertain how differences in the model physics and implementation (coding) affect the final model output. While working together on this task, these groups pursued different strategies for the comparison: Dr. Wang chose to compare the FASCODE and LBLRTM radiances to ground-based radiation measurements (ref), while the AER group focused on differences in the calculated optical depths.

There are several differences between FASCODE and LBLRTM that should be examined before discussing the simulation studies. First, the sub-Lorentzian component of CO₂ lines is treated differently. This gives rise to numerical differences which are particularly noticeable near the CO₂ bandhead, around 2380 cm⁻¹, and one would expect poor agreement between the models in the (approximate) region from 2375 - 2400 cm⁻¹.

The implementation of line coupling, as detailed in Section 4.3, is also different between FASCODE and LBLRTM. The coefficient values in LBLRTM were computed from theory. These coefficients were compared with measurements and scaled by 30% to agree with the data. This scaling is not inconsistent with the calculations because it is within the uncertainty of the variables in the calculations.

Another difference, which may in fact be the most important difference between the models, involves the monochromatic spectral resolution (DV), the average Lorentz halfwidth (ALFALO), and the maximum halfwidth (ALFMAX). The default value of ALFALO was changed from 0.08 cm⁻¹ in FASCODE to 0.04 cm⁻¹ in LBLRTM because 0.04 cm⁻¹ is a more reasonable number for most atmospheric calculations. The value of ALFALO impacts the resolution (DV) which is defined as the average Voigt halfwidth (ALFV) divided by the number of samples per mean halfwidth:

$$DV = \frac{ALFV}{SAMPLE} \quad \text{Eq. 6}$$

where ALFV is a function of both the Doppler and Lorentz halfwidths. Changing the value of ALFALO by a factor of two results in (almost) a factor of two change in the DV and increases the number of spectral points in the LBLRTM calculation over that of FASCODE. Advances in computer memory and speed since the original development of FASCODE means that increasing the number of spectral points does not significantly affect the calculation time, as it did when 0.08 cm⁻¹ was originally chosen.

Because ALFALO was changed, NBOUND also needed to be changed by a factor of two in order to keep ALFMAX the same:

$$ALFMAX = NBOUND * \frac{DV}{2} * \frac{1}{HWF3} \quad \text{Eq. 7}$$

$$NBOUND = 2 * (2 * HWF3 * SAMPLE + 0.01) \leftarrow FASCODE \quad \text{Eq. 8}$$

$$NBOUND = 4 * (2 * HWF3 * SAMPLE + 0.01) \leftarrow LBLRTM \quad \text{Eq. 9}$$

While ALFMAX remains the same after these changes, there is still a factor of two difference in the value of DV. This difference between the two models can produce major differences in the shape of the spectrum: DV is a part of the criteria for line rejection and with a smaller DV more lines will remain in the final calculation. However, two other parameters, DPTMIN and DPTFAC, also influence line rejection. Setting these parameters equal to zero will ensure that neither program rejects any lines.

Another aspect of the difference in DV is that the monochromatic spectra from FASCODE and LBLRTM will be written to TAPE12 at different spectral resolutions. For easy comparison of the two models one would like to have the same resolution. One hesitates to use a scanning function to change the DV to the same value in order to avoid introducing numerical effects into the computed spectrum. Further, it is important that the user not use the DVSET option as this will fix the DV during the calculations and can introduce distortions to the shape of the spectrum. Instead, for direct comparison of LBLRTM and FASCODE one should simply interpolate the final LBLRTM output (which is at higher resolution) to the resolution of FASCODE. This can be done using the INTRP subroutine or, when computing optical depths, LBLRTM can be instructed to interpolate the output to a specified DV without changing the DV used in the calculation (via the subroutine PNLINT and the control flag DVOUT).

Thus, in order to make meaningful comparisons of the two models one should (a) use the default values for ALFALO, and (b) set DPTMIN and DPTFAC to zero. This will result in the DV being different by a factor of two, but no lines will be rejected. The LBLRTM spectra can then be degraded to the FASCODE resolution for easy comparison.

A minor change in the default values of several parameters was also noticed. The default values for AVTRAT, TDIFF1, and TDIFF2 were changed from 2.0, 8.0, and 12.0 in FASCODE, to 1.5, 5.0, and 8.0 in LBLRTM. These parameters control the maximum Voigt width ratio across a layer, and the maximum allowable difference in temperature across the layers. Decreasing the sizes of these parameters causes an increase in the number of layers used in the calculation of the atmospheric path. This can provide a more accurate description of the atmosphere at the expense of increased computation time.

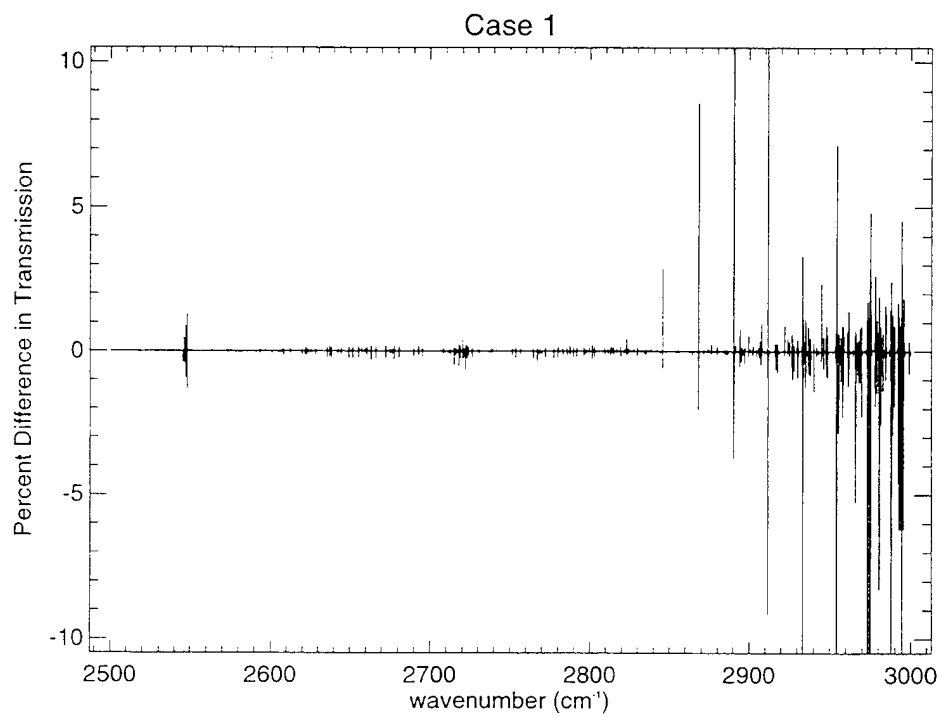
In order to remove extraneous features of the models, which can complicate the determination of differences between FASCODE and LBLRTM, the comparisons were based

solely on the computation of transmission for a single atmospheric layer. This was accomplished for three different layers selected to represent regions of predominately Lorentz broadening, Doppler broadening, and an intermediate case. Further, only the first seven molecular species from the HITRAN database were used, and the column density for each of the molecules was put into the TAPE5 file to eliminate differences in layering and the calculation of molecular amounts. Cross-sectional and continuum data were not included; and the value for ALFALO was set to the default value, even in line-coupling regions. These cases correspond to conditions defined by the US Standard Atmosphere. Specific characteristics of the cases are summarized in Table 5.

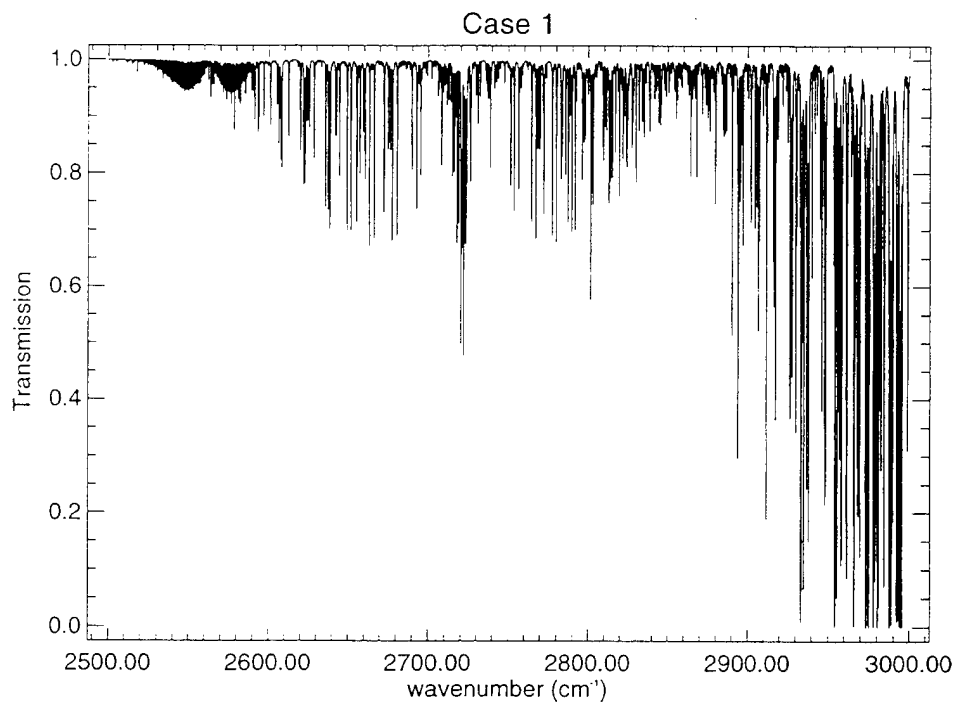
Table 5 Parameters for FASCODE/LBLRTM Comparisons

	Case 1	Case 2	Case 3
Pressure (mb)	972.2107	130.4209	0.1251
Temperature (K)	285.9446	216.7000	235.9188
H2O (cm-2)	1.231E+22	6.600E+18	3.810E+15
CO2 (cm-2)	5.696E+20	3.540E+20	2.928E+17
O3 (cm-2)	4.749E+16	6.434E+17	6.719E+14
N2O (cm-2)	5.524E+17	3.176E+17	1.424E+12
CO (cm-2)	2.559E+17	4.745E+16	1.487E+14
CH4 (cm-2)	2.934E+18	1.730E+18	1.331E+14
O2 (cm-2)	3.608E+23	2.242E+23	1.854E+20
All Others (cm-2)	1.349E+24	8.514E+23	7.281E+20
Layer Location (km)	0.0 - 0.7	13.4 - 15.9	62.9 - 65.3
Approx. Spectral DV (cm ⁻¹)	2.0E-02	3.0E-03	4.0E-04

Because of various array-sizes in FASCODE, the maximum spectral region over which a calculation can be done is 520 cm⁻¹. Hence, five separate runs of 500 cm⁻¹ regions were required in order to cover the entire spectral range from 500 - 3000 cm⁻¹. The results of selected cases in this spectral region are shown in Part (a) of Figure 4 through Figure 6 as the difference in transmission between FASCODE and LBLRTM. For information, Part (b) of these figures illustrates the absolute transmission for the layer computed by FASCODE and is useful in determining optically thick or thin regions of the spectrum to better gauge the magnitude of the errors.

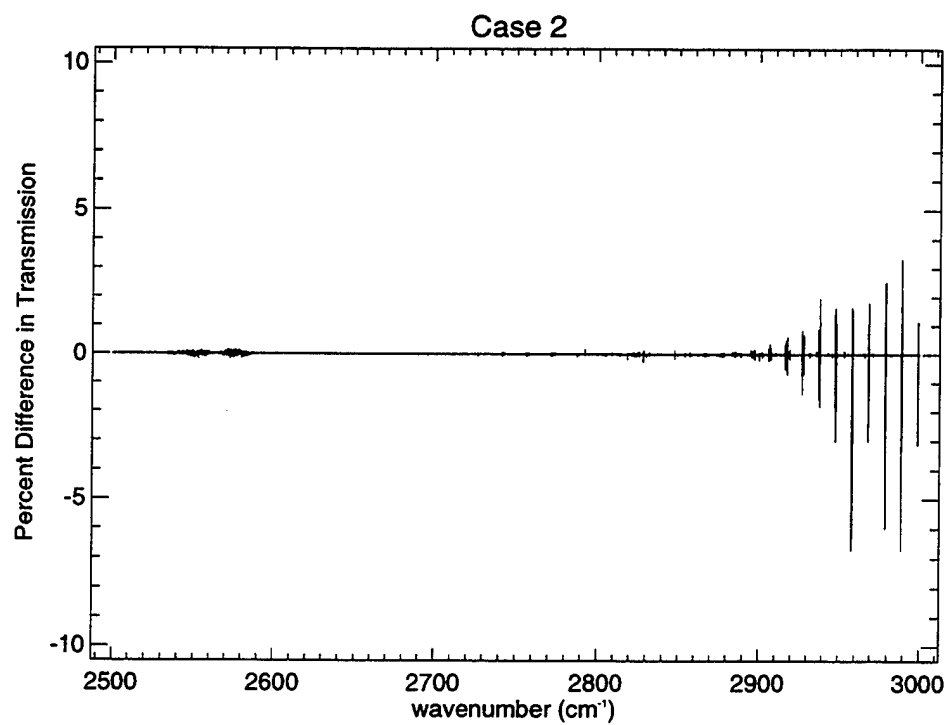


(a)

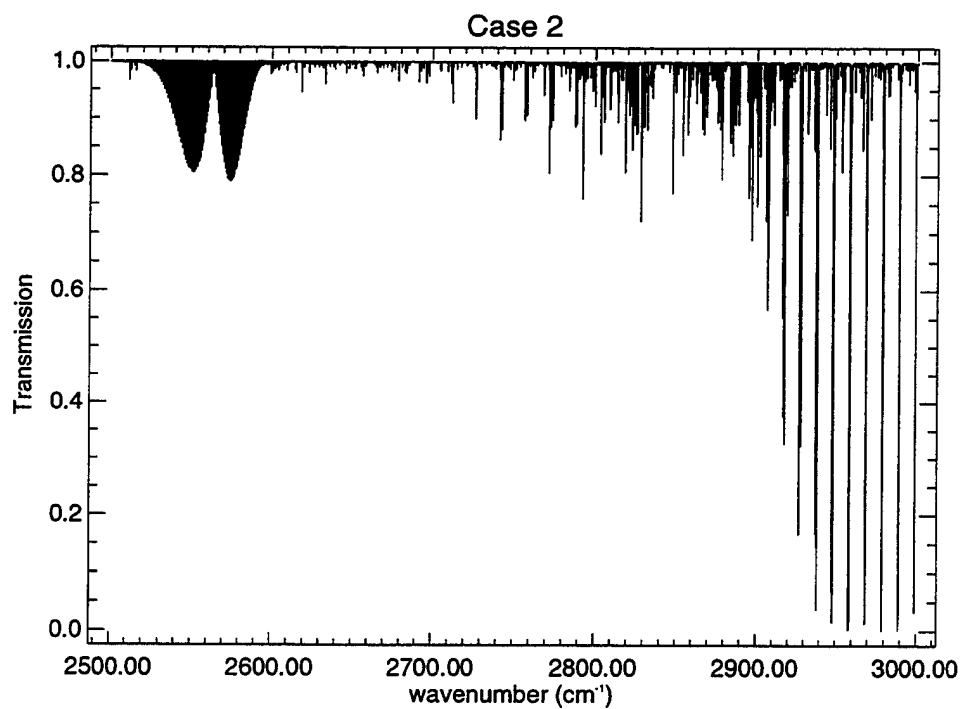


(b)

Figure 4 Comparison of FASCODE and LBLRTM Transmission for CASE1: $p=972.2107$, $T=285.9446$

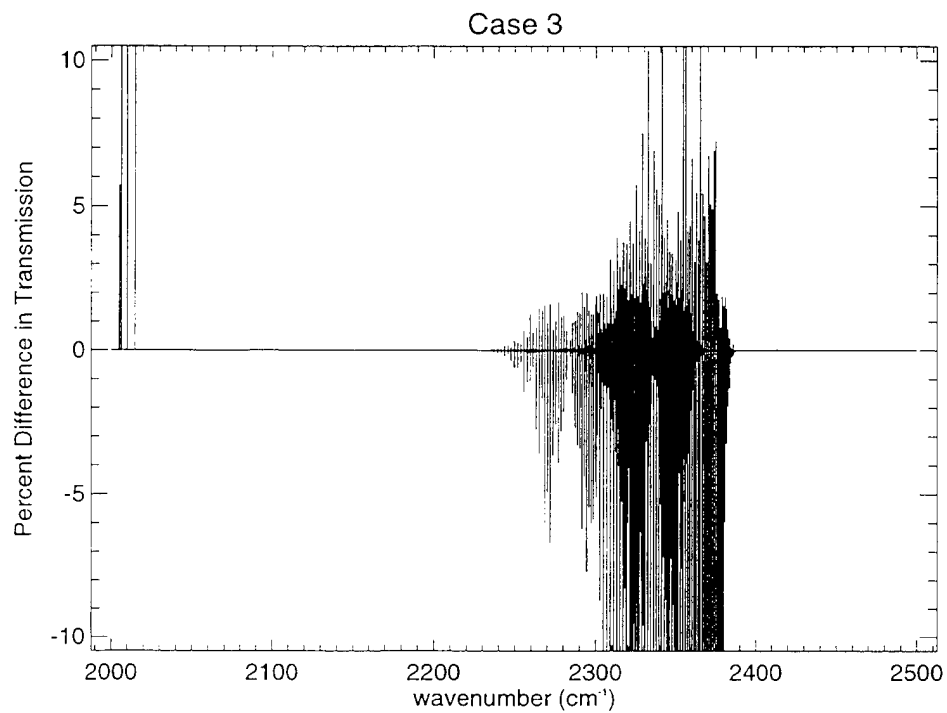


(a)

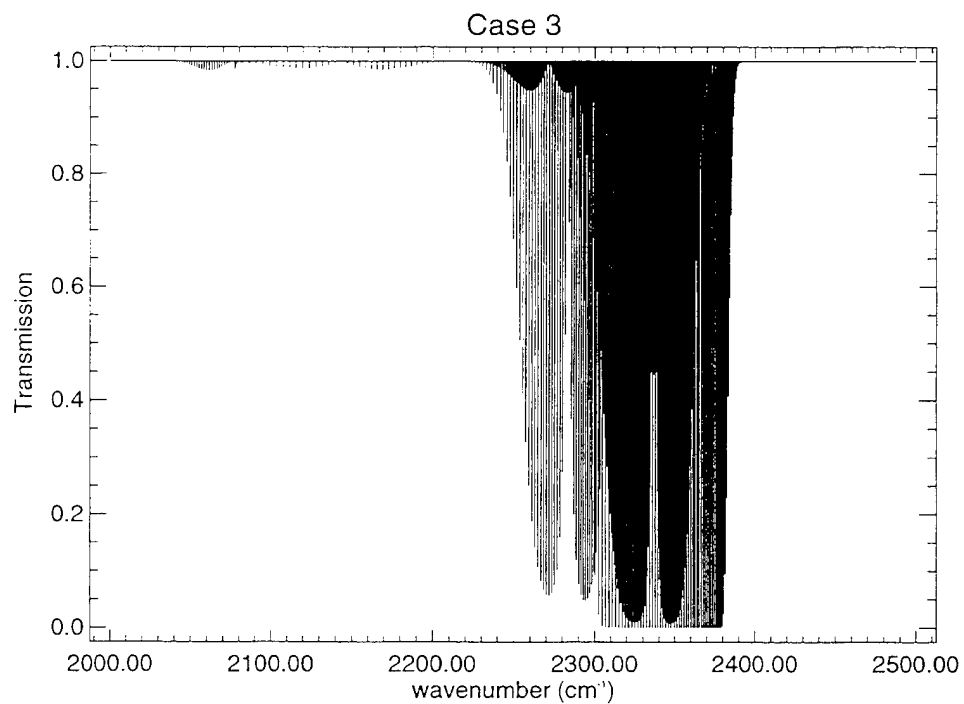


(b)

Figure 5 Comparison of FASCODE and LBLRTM Transmission for CASE2: $p=130.4209$, $T=216.7$



(a)



(b)

Figure 6 Comparison of FASCODE and LBLRTM Transmission for CASE3: $p=0.1251$, $T=235.9188$

In general, the results indicate that FASCODE and LBLRTM agree to within a few percent in transmission, which corresponds to less than 0.1% in optical depth. The largest differences among Figure 4, Figure 5, and Figure 6 occur at the center of absorption features. In order to understand the cause of these differences, spectral lines were examined individually. In doing so, it was found that differences in optical depth might be caused by the way the models compute the lineshape. To reduce computation time, both models compute the Voigt lineshape using an accelerated convolution algorithm (Clough, et al., 1981) which decomposes the line shape into four functions. This algorithm, described in Section 2.1.1, was changed for LBLRTM increase the accuracy of the calculation as compared to measured spectra (Clough and Brown, 1994). The transmission differences seen in this study, which are usually less than 1% in optical depth, can be attributed to the change in the Voigt function. As illustrated in the next section, these differences have little effect on the calculation of radiance or transmittance.

2.3. Conclusions

From the code comparisons and simulation results discussed above, we concluded that the best place to begin the FASE model would be from LBLRTM, since it already has the most of the features listed in Table 1. The main features it lacks are the non-LTE capability and the internal multiple scattering option. However, it is easier to put these back into the model than to reintroduce the other features back into FASCODE. Therefore the baseline FASE model has all the LBLRTM features listed in Table 1. Further modifications were made to FASE to upgrade existing features and to introduce new ones. These improvements are discussed in the following sections.

3. Upgrades to Existing Features

This section discusses upgrades to features already existing in the baseline version of FASE. Some of these upgrades fix errors in existing code, while others are extensions or improvements.

3.1. Geometry Routines

This section describes changes that were made to the line-of-sight geometry routines. As an introduction we provide a brief overview of the input parameters and how the package computes the final parameters. We then describe problems that are encountered using the old routines and how these problems have been solved for FASE. This work closely follows changes, which were made to the MODTRAN (Anderson et al. 1994) geometry package, as detailed in the report of Acharya et al. (1993). Because MODTRAN uses the same geometry package as FASCODE, and changes designed for one code can be readily ported to the other code.

3.1.1. Input/Output Module

The TAPE5 input file will accept various combinations of six parameters as well as a flag for indicating the type of path. These parameters are listed in Table 6. The path described by setting ITYPE = 1 has not been found to have problems and will not be discussed here. Paths described by ITYPE = 3 are a special case of the ITYPE = 2 path and thus will be covered by changes in the geometry.

Table 6 TAPE5 Input Parameters

Parameter	Definition
H1	Observer Altitude
H2	Source Altitude
ANGLE	Zenith Angle at H1
BETA	Earth-centered Angle (H1 to H2)
RANGE	Line-of-Sight Distance (H1 to H2)
ITYPE = 1	Horizontal Homogeneous Path
ITYPE = 2	Path from H1 to H2
ITYPE = 3	Path from H1 to Space

For the ITYPE = 2 specification there are four possible combinations of input parameters. These are listed in Table 7. The ultimate goal of the geometry package is to convert the input

parameters into the starting point (H1, which is always known), the ending point (H2), the viewing angle, and the minimum point along the path. Thus, all paths are eventually converted to the Case 2A specification: Case 2B is converted to 2A by determining H2; Case 2C is converted to 2D by computing the earth-centered angle BETA; and Case 2D is converted to 2A by determining the angle.

Table 7 ITYPE=2 Input Parameters

Case Designation	Input Parameters
2A	H1, H2, ANGLE
2B	H1, ANGLE, RANGE
2C	H1, H2, RANGE
2D	H1, H2, BETA

3.1.2. Identification of Existing Deficiencies

Differences between the path specified by the input parameters and the computed line-of-sight path are indicative of numerical problems within the geometry routines. As indicated in the report of Acharya et al. (1993) the inaccuracies can be attributed to the following:

1. Numerical precision problems
2. Calculation of H2 without including refraction (Case 2B)
3. Convergence problems for calculation of BETA (Case 2C & 2D)
4. Short slant paths

The solutions to these problems are discussed separately in the following sections. In addition to these changes, it should be noted that an attempt was made to make code easier to read by eliminating a number of "GOTO" statements.

3.1.3. Resolution of Deficiencies

3.1.3.1. Numerical Precision

Many of the equations used in the computation of the geometry involve R_e , the radius of the earth. This has the potential for introducing numerical errors since R_e is usually three orders of magnitude larger than the values of H1 and H2. In order to increase the precision of these calculations without using double precision variables, equations that include R_e were re-written in more appropriate forms. For example, the expression:

$$R_2^2 + R^2 - R_1^2 \quad \text{Eq. 10}$$

can be reformulated as

$$H_2^2 - H_1^2 + R^2 + 2R_e(H_2 - H_1) \quad \text{Eq. 11}$$

since

$$R_i = R_e + H_i \quad \text{Eq. 12}$$

It was confirmed that the numerical result of Eq. 11 is the same as using double precision with Eq 12. Another example of algebraic reformulation involves trigonometric identities:

$$R_2^2 + R_1^2 - 2R_1R_2 \cos\beta \quad \text{Eq. 13}$$

becomes

$$(H_1 - H_2)^2 + 4R_1R_2 \sin^2\left(\frac{\beta}{2}\right) \quad \text{Eq. 14}$$

3.1.3.2. Addition of Refraction for Calculation of Source Altitude

In the original geometry routine H2 was computed from H1, ANGLE, and RANGE by assuming straight-line geometry. This introduces errors that are especially large when the zenith angle is close to 90° and the range is large. To solve this problem a set of routines was added that include refraction in the determination of H2. This is accomplished through an iterative procedure, which computes the line-of-sight path length and compares it with the desired range. The routine converges to the correct value for H2 when the computed range is equal to the length of the input range. As a test of the accuracy the range was re-computed given H1, H2, and ANGLE. The results obtained before and after these changes were made to the code were compared with the results obtained using MODTRAN2, and are discussed below. We did not adopt the approach of MODTRAN2 and change all of the geometry routines into double precision. However, in order to converge to the results of MODTRAN2 it was necessary to change several subroutines to double precision. Further, many variables within other subroutines were also changed to double precision. These additional subroutines and changes are outlined in Table 8.

Table 8 New and Modified Routines

New Routines:	NEWH2
	RTBIS
	FNDPTH
Double-Precision Routines:	FINDSHDP
	SCALHTDP
	ANDEXDP
	RADREFDP
Changed Routines:	RFPATH
(some changes to double precision)	ALAYER
	FNDHMN

3.1.3.3. Short Slant Paths

The report of Acharya et al. (1993) recommended a new algorithm (based on the Newton-Raphson iteration method) for the calculation of BETA. While the implementation of this MODTRAN2 routine should have been straightforward, this was not the case. Due to slight numerical differences between MODTRAN and FASE the routine would not converge to the correct solution. In the end it was decided that the old "FDBETA" routine coupled with the algebraic and double-precision modifications discussed in Section 3.1.3.1 was sufficiently better than the original geometry package. Similarly, no modifications were made to improve the outputs for short slant paths.

3.1.3.4. Refractive Index Profile

In the course of validating the changes to the geometry it was noticed that MODTRAN2 and FASE use different formulations for the index of refraction. Further investigation showed that both formulations are based on the paper by Edlen (1966). The formulation in FASE (and FASCODE and LBLRTM) was originally coded for LOWTRAN and is presented in the report for LOWTRAN5 (Kneizys et al., 1980). This formulation is the simplification of Edlen's expression. Apparently the simplification was dropped in LOWTRAN6 in favor of the actual expression (Kneizys et al., 1983), and thus was employed in MODTRAN. While the profiles exhibit only slight differences these are sufficient to cause small deviations in the final line-of-sight path, especially for cases where refraction is significant. Since the LOWTRAN5 expression is a simplification to the exact expression we have dropped it from the coding in favor of the exact expression (this change was also made in the subroutine XAMNTS). We do not anticipate that this change will require the revalidation of FASE with other models or measurements.

3.1.4. Validation of Geometry module

In order to gauge the impact of the coding changes, comparisons were made between the "new" FASE geometry, the "old" FASE geometry, and the MODTRAN2 geometry. The results of these comparisons are shown in Table 9 for Case 2A, Table 10 for Case 2B, and Table 11 for Case 2C/2D.

Case 2A modifications consisted of the reformulation of equations and the changing of some variables to double precision. Therefore, one would not expect large differences between the old and new geometry. Table 9 illustrates changes to the value of phi, the zenith angle at H2 (used in the calculation of the refracted path), as a result of the new coding. The coding changes had little impact on the final results.

Table 9 Case 2A Model Comparisons for Geometry

H1	H2	ANGLE	PHI (old)	PHI (new)	HMIN (old)	HMIN (new)
20	100	90.1	99.0120	99.0120	19.9902	19.9901
		90.5	99.0252	99.0252	19.7518	19.7521
		91	99.0663	99.0663	19.0059	19.0057
60	100	90	96.3737	96.3737	60.0000	60.0000
		90.1	96.3745	96.3745	59.9902	59.9900
		90.5	96.3932	96.3932	59.7549	59.7551
		91	96.4514	96.4514	59.0205	59.0206
		95	98.0945	96.0945	35.5166	35.5167
		96	98.7450	98.7450	24.7101	24.7101

Larger differences between the old and new geometry are apparent for Case 2B, shown in Table 10. The largest errors in the old geometry occur when the refraction is largest, at viewing angles close to 90°. Also, the new geometry will give results for the case of a 90° viewing angle, while MODTRAN returns an error message.

Table 10 Case 2B Model Comparisons for Geometry (N,O = new,old FASE, M = MODTRAN; for PHI = 90° MODTRAN2 is unable to find the tangent point)

Model	H1	ANGLE	RANGE	H2	PHI	RANGE
N	5	92	10	4.65794	88.0803	10.01368
M				4.65794	88.0803	10.00394
O				4.65869	88.0794	9.97758
N	5	92	50	3.42779	88.3960	50.0190
M				3.42779	88.3959	50.0214
O				3.45068	88.3887	49.1827
N	5	92	100	2.19749	88.78511	100.0631
M				2.19743	88.7849	100.04798
O				2.29346	88.7495	95.5356
N	5	92	500	4.46282	91.8740	503.416
M				4.49087	91.8811	504.337
O				7.15381	92.4470	574.756
N	5	89	10	5.18148	91.0812	10.00415
M				5.18149	91.0812	10.00076
O				5.18213	91.0799	10.02902
N	5	89	50	6.04695	91.4015	49.9906
M				6.04695	91.4015	49.9993
O				6.06836	91.4078	50.8677
N	5	89	100	7.44533	91.8068	99.9934
M				7.44527	91.8068	99.9978
O				7.52881	91.8271	102.6277
N	5	89	500	31.8327	95.2424	499.9550
M				31.8336	95.2422	499.9918
O				33.2676	95.3797	515.4590
N	5	90	10	5.00715	90.0947	10.16462
O				5.00781	90.0862	10.60430
N	5	90	50	5.17290	90.3990	49.9615
O				5.19580	90.4229	53.0766
N	5	90	100	5.62983	90.7967	99.9713
O				5.78418	90.8484	106.150
N	5	90	500	22.7348	94.1480	499.950
O				24.5737	94.3697	523.980

The results for Case 2C/2D, shown in Table 11, also represent an improvement over the old routine, which would not converge at all for the case shown.

Table 11 Case 2C/2D Model Comparisons for Geometry (H1=H2=5km)

Input Range	Output Range FASE	Output Range MODTRAN	Output Range MODTRAN2
300	300.044	300.13	300.01
200	199.869	199.96	200.01
100	100.3059	100.52	100.01
50	49.6897	50.51	50.02
20	19.8501	-	20.01
10	9.35703	9.20	10.02
8	8.10367	7.51	8.01
6	-	7.51	6.01
4.7	-	-	4.72
2.01	0.0	5.31	2.00

Table 12 summarizes the geometry test results for FASE, MODTRAN2, and FASCOD3P. For this test H1 = 5.0 km, Range = 10 km, and H2 was varied as indicated in the table. Given H1, H2, and Range the geometry package will first calculate the earth-centered angle ("PHI") and then the H1-H2 viewing angle ("ANGLE"). The numbers tabulated are the range computed after finding the viewing angle (and should be equal to the input range of 10 km). Except for Test 2, the new FASE geometry is much better than the old FASCOD geometry. However, as noted in the Version 1.0 report, there are still some differences relative to MODTRAN.

Further examination of these test cases indicates that the differences between FASE and MODTRAN are the result of slight numerical differences.

Table 13 shows the values of PHI (the zenith angle at H2 used in the calculation of the refracted path), ANGLE (the viewing angle at H1), and HMIN (the computed tangent point along the path from H1 to H2). "RANGE DIFF" refers to the difference in the range computed with FASE and MODTRAN2 as given in Table 12; "PHI" is the earth-centered angle; "ANGLE" is the H1-H2 viewing angle; and "HMIN" is the computed tangent point of the refracted path. The results of Test 3 clearly show that just a slight change in the calculation of the viewing angle will affect the final calculation of the range.

Table 12 Case 2C Geometry Test Results

TEST	H2	FASE	FASCOD3P	MODTRAN2
1	6.0	10.001	10.008	10.008
2	5.5	10.007	10.005	10.017
3	5.25	10.012	10.024	10.014
4	5.0	9.357	11.837	10.014
5	5.01	10.335	no convergence	10.009
6	5.007	10.234	9.547	10.021
7	5.001	no convergence	no convergence	10.014
8	5.0015	10.219	no convergence	10.013

Table 13 Values Computed to Define Path Geometry

TEST	RANGE DIFF		FASE	MODTRAN2
3	0.002	PHI	91.470	91.471
		ANGLE	88.609	88.609
		HMIN	5.000	5.000
5	0.326	PHI	90.096	90.097
		ANGLE	89.986	89.983
		HMIN	5.000	5.000
8	0.206	PHI	90.048	90.049
		ANGLE	90.037	90.031
		HMIN	4.999	4.999

In summary, the results of the validation study indicate that the new geometry package is a significant improvement over the existing routines and solves many of the problems that have been encountered. Further changes to the geometry to improve Case 2C/2D, especially for short input ranges, will be considered for future versions of FASE as time permits.

3.2. Chappuis And Wulf Ozone Bands

The coefficients for the ozone Chappuis band were updated to the values found in MODTRAN3 (Shettle and Anderson, 1995). These coefficients include both the Chappuis and Wulf absorption and cover the range from 9170 to 24565 cm^{-1} . The coefficients at each wavenumber are now given for a quadratic polynomial that is a function temperature:

$$C(\nu) = X(\nu) + Y(\nu)\Delta + Z(\nu)\Delta^2 \quad \text{Eq. 15}$$

where

$$\Delta = T - 273.15 \quad \text{Eq. 16}$$

and T is the average temperature. The coefficients are specified at intervals of 5 cm^{-1} .

The original coefficients were valid over the temperature range 220 - 298 K. This was extended to 180 - 310 K to cover the range of temperatures typically encountered in atmospheric applications. Further, an extrapolation was done at the edges of the data to eliminate edge effects caused by a sudden decrease of the coefficients to zero value.

3.3. Non-Local Thermodynamic Equilibrium (NLTE)

One of the larger projects in converting LBLRTM into FASE involved the conversion of the FASCODE NLTE routines into a format compatible with the LTE portion of the code (panel structure, common blocks, array dimensions, etc.). Prior to making this conversion, several differences between the LTE and NLTE routines of FASCODE were identified and eliminated (by Jim Chetwynd of the Air Force Phillips Laboratory) so that a calculation using only LTE spectral lines will achieve the same answer regardless of whether the LTE or NLTE routines were used. Once these changes were made to FASCODE, the sections of code relevant to NLTE calculations were identified. These sections were then added to the FASE subroutines to create a parallel version of HIRAC for NLTE calculations.

3.4. Black-Body Approximation

At the October 1994 ARM Science Team meeting it was shown that there were problems in the LBLRTM output when doing calculations with aerosols, as evidenced by a "step function" radiance profile rather than a smooth curve (Anderson, 1994). We worked directly with the LBLRTM team at AER to identify the cause of these problems and to re-code the necessary sections of the model. It was found that the step-function was the result of improper interpolations of the blackbody function as a part of the Padé approximation. This error was related to another problem in which LBLRTM did not properly include the surface emissivity. We have corrected these sections of the code in both FASE and LBLRTM.

3.5. Emissivity/Reflectivity

Previous versions of FASE, FASCODE, and LBLRTM give the option of specifying the boundary emissivity and/or reflectivity. This is accomplished through the use of quadratic coefficients to specify the spectral signature of the boundary. However, a quadratic formulation

is not sufficient for all simulation scenarios since the emissivity or reflectivity can have a non-uniform spectral distribution (e.g., the sea-surface emissivity). To rectify this problem we have included the option of putting the emissivity and reflectivity coefficients in data files. This is similar to an option that was added to MODTRAN. To use this option, set the first coefficient (SREMIS(1) and/or SRREFL(1)) equal to -99 and the other two coefficients equal to zero. This will signal FASE to look for the files "EMISIV.IN" and/or "REFLEC.IN".

3.5.1. Input File Format

The format for the emissivity and reflectivity files is the same. The first line contains header information that will be written to the TAPE6 output file. The second line gives the starting and ending wavenumbers for the file as well as the number of points in the file. The user may set the starting wavenumber to be less than zero to signify that wavenumber-coefficient pairs are specified, otherwise it is assumed that the coefficients are spaced equally between the starting and ending wavenumbers. The remaining lines in the data file contain the coefficients or wavenumber-coefficient pairs. These are listed with six values per line (or three pairs if the wavenumber option has been selected). This file structure is summarized below:

line 1: 80 character header (for user information only - written to TAPE6)

line 2: V1, V2, NPTS (E13.6, E13.6, I4)

V1 = starting wavenumber of data

V2 = ending wavenumber of data

NPTS = number of data points in file (max = 2000)

line 3 - n: coefficients (6(E11.4,2X))

coefficients are listed with six values per line, with equal wavenumber spacing between the coefficients

if V1 < 0 in line 2, the wavenumber-coefficient pairs are expected and there are three pairs per line

3.6. Hartley-Huggins Continuum / Herzberg Continuum

An error in the array dimensions for the Hartley-Huggins (O₃) continuum absorption data statements was identified and corrected.

The pressure-dependence correction routine for the Herzberg (O₂) continuum cross-sections has been modified to reflect a more recent formulation (Anderson et al., 1990). The pressure dependence proportionality constant was changed from 1.72E-03 (at 760 torr and 273.15 K) to 1.81E-03 (at 760 torr and 293.15 K). The net result, after converting to 273.15 K and including the O₂ and N₂ mixing ratios, is a change from 0.73 to 0.83 in the factor modifying the pressure/temperature scaling term.

3.7. Absorption Cross-Sections

A number of "go to" statements in the subroutine "XSECTM" were changed to avoid an error whereby all remaining cross-section files would be skipped if it was found that the current file does not have any lines in the spectral region of interest. It was also discovered that some array indices were incorrectly coded after allowing for the option to input cross-sections with pressure units of Torr.

3.8. Layer Input/Output Units

One of the options available is for the user to specify the layering scheme and provide the column amounts within each layer for the molecules of interest. We have extended the allowed input units to include "atm-cm". If this option is selected the input amounts are converted directly to molecules cm^{-2} ; without this option the input is assumed to be molecules cm^{-2} unless the value is less than 1.0 in which case it is assumed to be mixing ratio. With the mixing ratio option the column amount for the broadening gas must still be input in molecules cm^{-2} , while for the atm-cm input **all** of the amounts must be in atm-cm.

Using the IPUNCH = 1 option (TAPE5, record 3.1), layer information written to TAPE6 will now include the units of atm-cm.

3.9. Laser Calculations

As noted in Section 2.1.6, the 4-function line decomposition employed by FASCODE can introduce errors in the calculation of a specific frequency point, and the LASER option was devised to circumvent this for calculations over a very narrow spectral band. Since the laser option has been recoded for use in FASE, it was dropped from LBLRTM. This option allows the user to calculate only the narrow region around the laser frequency and print the results at the end of the TAPE6 output file. This option is signaled if V1=V2 in the TAPE5 input file. Calculations with the laser option were compared to calculations over a wide spectral region of radiance, transmittance, and optical thickness and were found to be in exact agreement.

4. New Features

This section describes new features added to FASE that were not contained in any of the previous FASCODE models or in LBLRTM.

4.1. Schumann-Runge Band and Continuum

Information about the O₂ Schumann-Runge band and continuum absorption was added to the continuum module of FASE. The data are polynomial coefficients from a fit devised by Minschwaner et al. (1992, 1995) and are valid from 49000 cm⁻¹ to 57000 cm⁻¹. The fit was accomplished on a 0.5 cm⁻¹ spectral grid using cross-sections obtained from a line-by-line radiative transfer model which included contributions from the temperature dependent Schumann-Runge continuum.

For a single layer the absorption cross-section at a particular wavenumber may be written in the form

$$S = Ax^2 + Bx + C \quad \text{Eq. 17}$$

where S has units of cm² and x is the "modified temperature", which is related to the average temperature of the layer, T:

$$x = \left(\frac{T - 100}{10} \right)^2 \quad \text{Eq. 18}$$

In order to achieve the proper dependence on temperature there are three sets of coefficients corresponding to three temperature regimes. These regimes are defined as:

$$\begin{aligned} 130 \text{ K} &\leq T < 190 \text{ K} \\ 190 \text{ K} &< T < 280 \text{ K} \\ 280 \text{ K} &< T < 500 \text{ K} \end{aligned}$$

For convenience the data are supplied in three ASCII data files (130-190.cf4, 190-280.cf4, and 280-500.cf4).

The cross-section coefficients are tabulated at intervals of 0.5 cm⁻¹. For three coefficients in three temperature regimes this corresponds to a total of 72000 values. Rather than place all of these values in "block data" statements, a program was written to convert the ASCII data files into an unformatted data file (SCHRUN.DAT) which can be read using the FASE I/O subroutine

"BUFIN". Because unformatted data is treated differently with different computers, FASE is distributed with ASCII data files and a conversion program.

The unformatted data file is written in a block structure consisting of a header and the corresponding data. The header contains the starting wavenumber of the block, the spectral spacing of the data, the number of points, and a flag signifying the temperature regime. Each block of data covers 400 cm^{-1} and, with three coefficients for each spectral point and a resolution of 0.5 cm^{-1} , each block contains 2400 points.

Within the continuum module the program chooses the correct temperature regime, reads the corresponding coefficients, and computes the cross-section as in Section 4.5. The result is interpolated to the appropriate spectral resolution and added to the array containing the continuum contribution to the total optical properties.

4.2. Solar Spectrum

A solar spectrum module was added to give FASE the capability of computing solar transmission through the atmosphere (which is particularly useful for simulations of experiments employing the technique of solar absorption spectroscopy). Ultimately the solar module could be combined with a multiple-scattering routine for a better treatment of the atmospheric radiation field. FASE is distributed with two solar spectrum files to cover the spectral range from $50 - 57490\text{ cm}^{-1}$.

The spectrum was supplied in SOL.RAD by Kurucz (1994). It is composed of three solar irradiance spectra collected by Kurucz, the Air Force Phillips Laboratory Geophysics Directorate (GL), and the SUSIM instrument which flew on the Space Lab 2 flight of the Space Shuttle (Hall and Anderson, 1991). The following details the method by which the data were converted to the spectrum supplied with FASE.

The Kurucz spectrum was given as the value of the solar irradiance at intervals of 1 cm^{-1} from 50 to 50000 cm^{-1} in units of $\text{ergs cm}^{-2}\text{ s}^{-1}(\text{cm}^{-1})^{-1}$. The irradiance was converted to the standard unit of $\text{watts cm}^{-2}(\text{cm}^{-1})^{-1}$, and the spectrum was then smoothed using a running three-point triangle, to make its excursions more similar to measured spectra in the ultraviolet. It should also be noted that toward higher wavenumbers the smoothing begins to have little effect, since the spectrum becomes naturally smooth.

The GL spectrum is a combination of 1978 data and 1983 data, normalized to 1983. Given in 0.02 \AA steps and was also smoothed by a 3-point triangle, it was then normalized to the SUSIM data from the Space Lab 2 flight using a 41-point smoothing of the ratio of the two spectra. The data were then converted from irradiance units of $\text{photons cm}^{-2}\text{ s}^{-2}\text{ \AA}^{-1}$ to $\text{watts cm}^{-2}(\text{cm}^{-1})^{-1}$ and interpolated to give values at equally spaced intervals of 1 cm^{-1} .

The Kurucz spectrum and the GL spectrum were then compared in the range of 32250-32350 cm^{-1} and a splice-point was chosen on an ascending flank in the range from 32288 to 32292 cm^{-1} , where the agreement was good for five points in a row. The composite spectrum is the smoothed Kurucz spectrum from 51 to 32290 cm^{-1} and the smoothed and interpolated GL spectrum from 32291 to 49983 cm^{-1} .

The second spectrum, SOL2.RAD, covering the range from 48560 to 57490 cm^{-1} is from SUSIM data. It has the same units and file structure as SOL.RAD.

4.2.1. File Structure

The solar spectrum data were initially supplied in a 2-column ASCII data file. This file is rather large (about 898 K) and the first step was to reduce it to a more manageable size. This was accomplished by converting it to a block format (still in ASCII). The blocks consist of a header denoting the starting wavenumber of the block, the spectral interval (1 cm^{-1}), and the number of points in the block (2400 for all except the last, which contains 1933 points). The irradiance data follows each header and is arranged with six values per line. (The very last line has one real point and five denoted "-99.9" to fill the line). Converting the data to this format reduces the file size to about 608 K.

As with the data for the Schumann-Runge band (Section 4.1) it is advantageous to read data from an unformatted data file. The user is supplied with the Kurucz solar spectrum in the block-ASCII format (SOL.ASC). A conversion program is supplied that will convert the block-ASCII file into an unformatted file (SOL.UNF) with the same structure (this program ignores the last five data values, "-99.9", to ensure that they are not inadvertently incorporated into FASE calculations). The unformatted file occupies about 200 kilobytes of disk space. The SOL2.UNF file is created with another conversion program converting block-data statements into an unformatted file.

Supplying the solar spectra in this fashion is advantageous to the user community since each user may easily use any solar data without converting it to a block-data statement and recompiling the program, thereby increasing the flexibility of FASE.

4.2.2. Implementation

Implementation of the solar spectrum is accomplished with Record 1.2 and Record 1.2b of the TAPES input file. The user has the choice of doing a 'normal' calculation and then incorporating the solar spectrum, or simply using previously calculated files. In order to do the complete calculation, IEMIT (Record 1.2) should be set equal to 2; IEMIT should be 3 to skip directly to the solar routines. With either case the filter, scan, and plot functions occur after the solar routines.

FASE requires that Record 1.2b follow Record 1.2 if IEMIT equals 2 or 3 (note that Record 1.2 is the first line after the header information). Record 1.2b contains three parameters (INSOLR, IOTSOL, and ISOLOC) which provide information about input and output files, and thus the type of merge that is to be done. If INSOLR equals 0 the input file is the radiance/transmittance file (TAPE12), while if it equals 1 the input file is the total optical depth file (TAPE10). With IOTSOL equal to 0 the merge produces only the attenuated solar radiation, while IOTSOL equal to 1 produces the total radiation field (the transmitted solar radiation plus the thermal emission). The output is always written to TAPE11. One should also recognize that if the total radiation field is desired, INSOLR must be equal to zero to provide the thermal emission term. The ISOLOC parameter is used to specify the location of the solar irradiance. If ISOLOC equals 0 (default), the solar irradiance is taken from the file SOL.UNF (or SOL2.UNF), while for ISOLOC equal to 1 the solar irradiance is read from TAPE24. The TAPE24 file is created by setting ISOLOC=1, as discussed in Section 4.2.3.

The merging of the solar radiance with the input information is accomplished as follows: If optical depth is input, the transmission is computed; the solar file is interpolated to the spectral resolution of the input file and the transmitted solar radiation is computed. Finally the thermal component is added (if desired) and the result is written to TAPE11.

4.2.3. Calculations with the Solar Irradiance Option

Calculations utilizing the solar irradiance option fall into two categories. The first is direct transmission where the observer is looking at the sun, either with a short, direct slant path or through a limb path. The other type of calculation is that of sunlight reflected off a surface into the line-of-sight.

Depending on the geometry of the problem, calculations with a surface reflectance can require multiple runs of FASE. For a downlooking calculation, FASE sets the top of the atmosphere to the observer altitude (H1) and computes both the upwelling radiance from the surface (H2) to the observer and the downwelling radiance from H1 to H2, reflected off the surface and attenuated back to H1. Whether or not this calculation is sufficient depends on the altitude of H1 and H2 (both relative and absolute) and the spectral band. In a weakly absorbing spectral region, the downlooking instrument at H1 may 'see' radiation that was emitted from above H1, attenuated down to the reflective surface H2, reflected and attenuated back to H1. These types of calculations can be done with FASE, but require varying degrees of setup by the user.

The downlooking case from H1 to a reflective surface H2 with no contribution to the radiance from the atmosphere above H1 can be run in the same manner as the direct transmission

case: set IEMIT=2, INSOLR=0, IOTSOL=0 or 1, and ISOLOC=0. One should note that the surface is treated as a Lambertian reflector for the purposes of the reflected solar irradiance.

A calculation that needs to include radiation emitted from above H1 must be done as two runs of FASE. For purposes of this discussion the observer altitude will be defined as Hobs, the surface altitude as Hsurf, and the top of the atmosphere (typically 100 km) as TOA. The first run, "run 1", should be set as for the uplooking direct transmission case: H1=Hobs, H2=TOA, IEMIT=2, INSOLR=0, IOTSOL=1, and ISOLOC=-1. This calculation will compute the attenuated solar plus thermal radiation from the top of the atmosphere to the observer altitude. The result will be written to the file TAPE24. The second run of FASE, "run 2", is set as for the downlooking case: H1=Hobs, H2=Hsurf, IEMIT=2, INSOLR=0, IOTSOL=1, and ISOLOC=1. This will complete the calculation by using the result from run 1 as the downwelling radiation reaching Hobs, which will then be attenuated to Hsurf, reflected, and attenuated back to Hobs.

4.3. Line Coupling

Line coupling is an important phenomenon that occurs in collisionally broadened spectra when the lines are very close together. While the theory will not be discussed in this report, the treatment of this phenomena in FASCODE / LBLRTM / FASE requires that all of the lines from a particular line coupling region be included in the calculation. The structure of FASCODE / LBLRTM assumes that the user recognizes this and adjusts the limits of the spectrum accordingly. For FASE a different strategy was adopted whereby the program checks to see if more lines need to be included in the calculation and adjusts the spectral limits as necessary. To avoid problems with output files, etc., this adjustment is transparent to the user and the output file retains the limits specified by the user. When this occurs a warning message is written to the screen and to the TAPE6 output file.

The implementation of this limit-checking scheme begins with the creation of the TAPE3 (spectral line data file) using the program LNFL. This program checks the line coupling coefficients (stored in data statements) and puts the limits of the various line-coupling regions in the TAPE3 header. If the user has selected a spectral range that starts or ends in a line coupling region, LNFL will modify the spectral limits to be sure that all of the coupled lines are selected.

For each atmospheric layer FASE determines the spectral range for which to retrieve lines from TAPE3. After this region is selected the subroutine CHKLNC will check the limits to see if they fall within a line-coupling region. A limit falling within a line-coupling region will be reset to four halfwidths beyond the region (where the halfwidth is taken to be the average halfwidth of the layer). Changing this limit will modify only the spectral range of the calculation and not the spectral range of the output file. This change has been made to both the LTE and NLTE portions of the code and the user is notified in the TAPE6 file if the limits were changed.

4.4. HITRAN96 Line Parameters

A new feature to FASE is that it accepts HITRAN96 line parameters. The code has been modified to accept 36 species from the HITRAN database as opposed to 32 species, as was the case with FASCOD3. The code was modified by changing dimension statements and partition function arrays to accommodate HITRAN96. It should be noted that not all of the molecules have internally stored profiles. For species for which there are no internally stored profiles the atmosphere must explicitly specified by the user as discussed in Section 4.5.4.

4.5. HITRAN96 Heavy-Molecule Cross-Sections

Laboratory measurements of the absorption properties of heavy molecules were recently made (e.g. Li and Varanasi, 1994; Varanasi and Nemtchinov, 1994, subsequently referred to as "Varanasi's cross sections") and are included on the 1996 release of the HITRAN databases (Rothman et al., 1992, 1996). Because of the complexity of these molecules and the fact that individual spectral lines cannot be resolved at temperatures and pressures typical of the earth's atmosphere, the measurements consist of relatively low spectral resolution information in the form of absorption cross-sections (i.e. without information about line strengths, positions, halfwidths, etc.). Many of these molecules have been included on previous versions of the HITRAN databases in that form, as temperature dependent cross sections rather than the traditional HITRAN format of line position, line strength, halfwidth, etc. However, the Varanasi measurements are provided as a function of pressure and temperature as opposed to the previous HITRAN format, which extrapolated the temperature-dependent values to zero pressure. To compute the optical depth for a particular (p,T) combination with the 'old' data, it was necessary to interpolate between temperatures while convolving with the appropriate Lorentz line shape for the pressure, finally combining this derived cross section with the density weighted path amounts. With the Varanasi data, one is required to interpolate and/or extrapolate between the tabulated data to arrive at the correct absorption coefficient. Thus, in order to accommodate this new data directly, it would be necessary to re-configure the FASE algorithms to bypass the convolution and perform the necessary interpolation and/or extrapolation. Further, one must develop an appropriate scheme for extrapolating the tabulated values to pressures and temperatures outside the range of the measurements.

One approach through which the Varanasi cross-sections may be utilized by the FASE algorithms is to perform a least-squares fit to the data with a series of spectral lines, solving for the line strength, halfwidth, and lower state energy (Toon, G., 1995). The pseudo-line approach incorporates all the (p,T) combinations of data into the least-squares fit and increases the accuracy from a simple interpolation between two (p,T) values. The pseudo-line data is easily

merged with the spectral data taken from HITRAN when creating the 'TAPE3' line file, and the radiative transfer calculations are performed as usual, with the model using the spectral line routines, rather than the cross-section routines, when computing the absorption of these species.

One drawback to the pseudo-line approach is that new sets of pseudo-lines are required as more molecules are added. In the long run it would be desirable to develop a scheme to use the cross-sections given as a function of pressure and temperature. Since the problem lies in interpolating/extrapolating the absorption coefficient data to specific values of the pressure and temperature, one might use the pseudo-line approach to fill out the full matrix of required pressures and temperatures (that is, use FASE to compute the absorption coefficients for the regions not represented by the measurements). For the time being it is sufficient to investigate the implementation of the pseudo-line approach and begin to explore ways in which the actual data can be used, perhaps in conjunction with 'pseudo-data' based on calculations with the pseudo-lines.

The pseudo-line approach has been evaluated using line data for CFC-12 from fits made by Toon (1995). Before this method can be accepted there are two questions that must be addressed: (1) does the calculation with the pseudo-lines accurately reproduce the measured absorption coefficients? (2) what is the timing impact of using the pseudo-lines compared to the (low spectral resolution) cross-sections? These are discussed in the following two sections. Section 4.5.3 outlines the coding changes required to implement the pseudo-line spectral information while Section 4.5.4 explains how one can do a calculation utilizing this data.

4.5.1. Accuracy of Pseudo-Line Approach

The accuracy of the pseudo-line approach was evaluated by computing the optical depth for a horizontal path with constant pressure and temperature and a single molecular species (CFC-12). The absorption coefficient, k , can be determined directly from the calculation:

$$k_{\text{calc}} = \frac{\tau}{N} \quad \text{Eq. 19}$$

where τ is the optical thickness, N is the absorber density integrated along the line-of-sight path and k has units of cm^2 . The calculated absorption coefficient can then be compared directly with the measurements in order to determine the validity of this approach.

This test was done for several different combinations of pressure and temperature as well as different absorption path lengths. Figure 7 and Figure 8 show the calculated absorption cross-section for F-12 for two different (p,T) combinations and a 1 km path. The percent difference between the computed cross sections and Varanasi's measurements are plotted in Figure 9 through Figure 12 for the 1 km and 50 km paths. Because of systematic differences in the wings

of the band, where the absorption is very small, only the region from 860 - 940 cm^{-1} is shown in the difference plots (note that the scales are different between Figure 9/Figure 10 and Figure 11/Figure 12). The systematic differences are clearly seen in Figure 13, a plot of the difference rather than percent difference, and Figure 24, where it can be seen that negative values for the data were set to zero. It is interesting to note that the percent difference over the region plotted in Figure 9 through Figure 12 is identical regardless of the length of the absorption path. The fact that the percent difference does not scale with path length indicates a consistency in the FASE calculation. Figure 14 through Figure 18 detail certain regions of Figure 7, while Figure 19 through Figure 23 detail regions of Figure 8. In these figures the computed value of the cross section (solid line) is compared with the data measured and reported by Varanasi (dotted line).

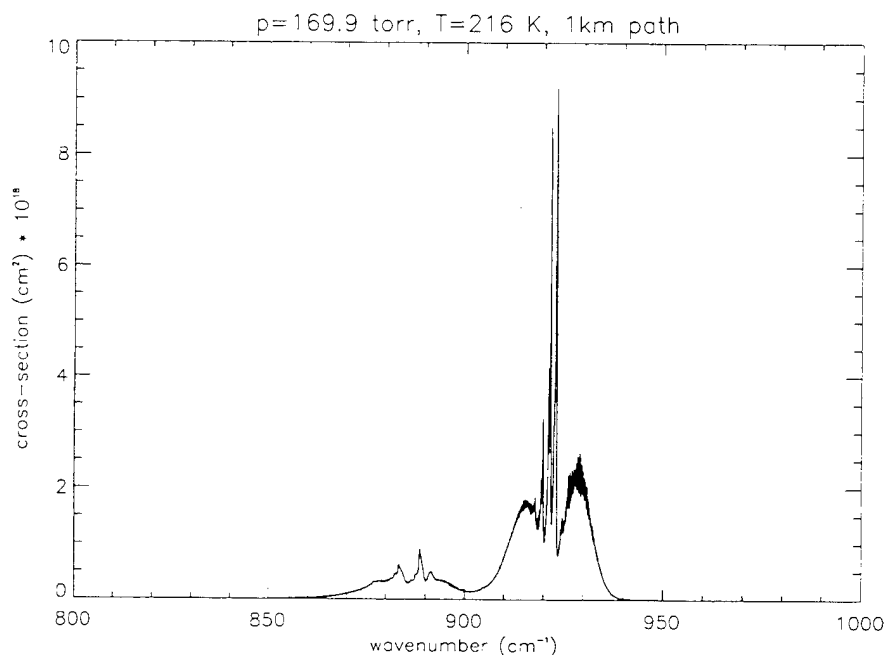


Figure 7 Absorption Cross-Section from the FASE Calculation for a 1km Path at $p=169.9$ torr, $T=216.0$ K (path amount of F-12= $1.814\text{E}+14$ molecules cm^{-2})

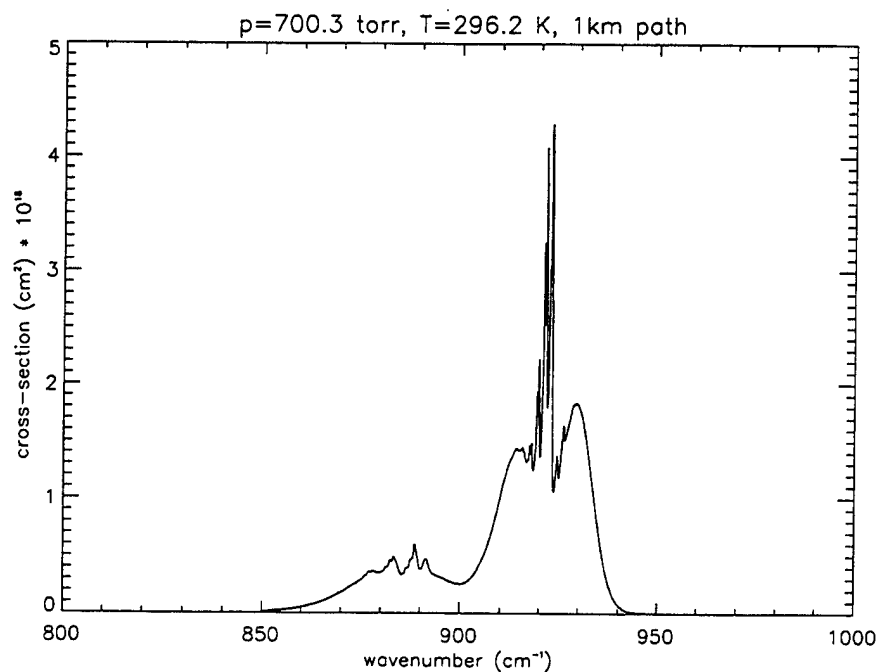


Figure 8 Absorption Cross-Section as Computed from the FASE Calculation for a 1km Path at p=700.3 torr, T=296.2 K (path amount of F-12=5.437E+14 molecules cm⁻²)

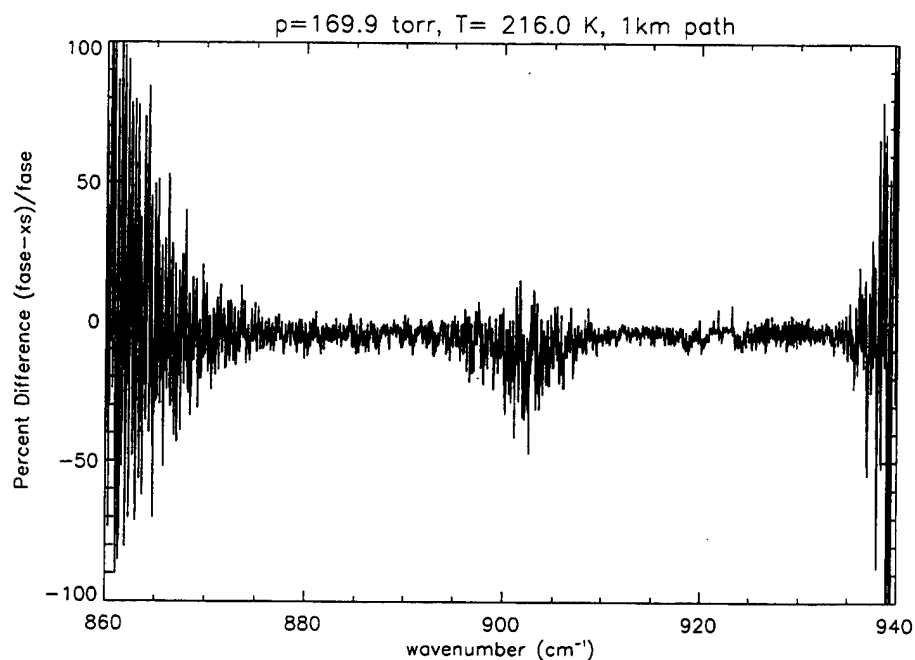


Figure 9 Percent Difference Between the Cross-Section Computed with Pseudo-Lines and the Data from Varanasi for a 1km Path at p=169.9 torr, T=216.0 K

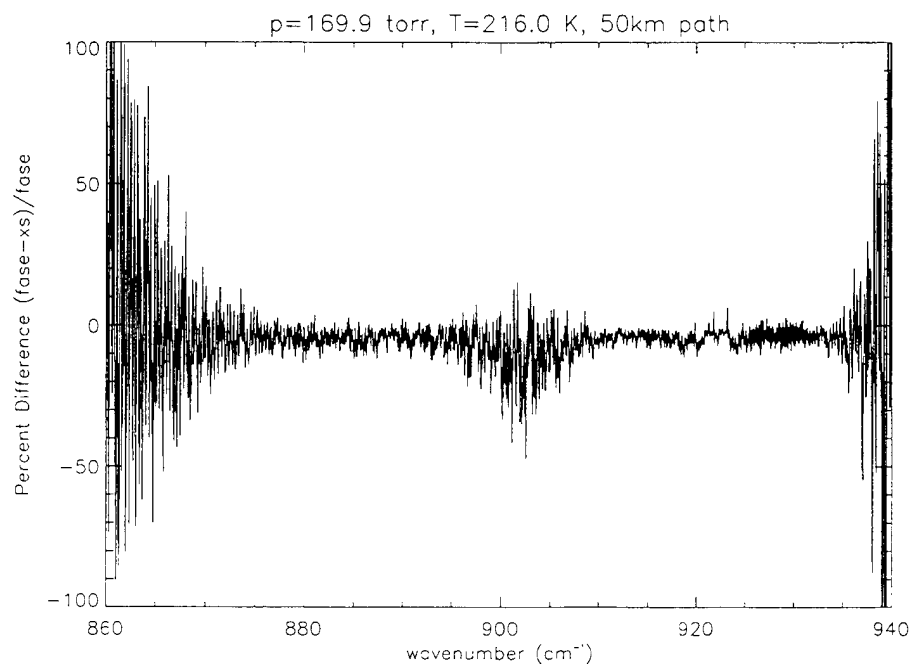


Figure 10 Percent Difference Between the Cross-Section Computed with Pseudo-Lines and the Data from Varanasi for a 50km Path at p=169.9 torr, T=216.0 K

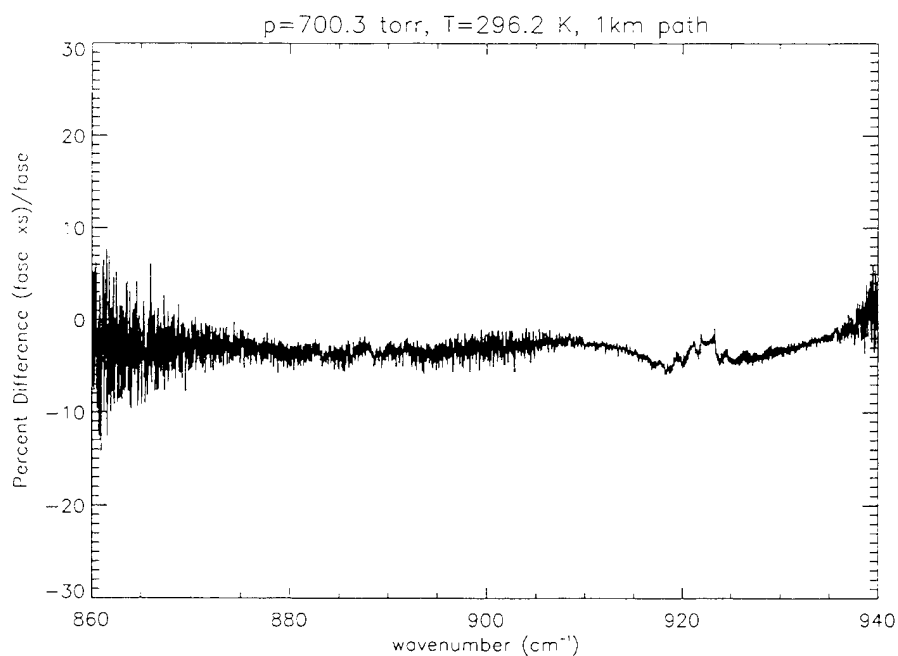


Figure 11 Percent Difference Between the Cross-Section Computed with Pseudo-Lines and the Data from Varanasi for a 1km Path at p=700.3 torr, T=296.2 K

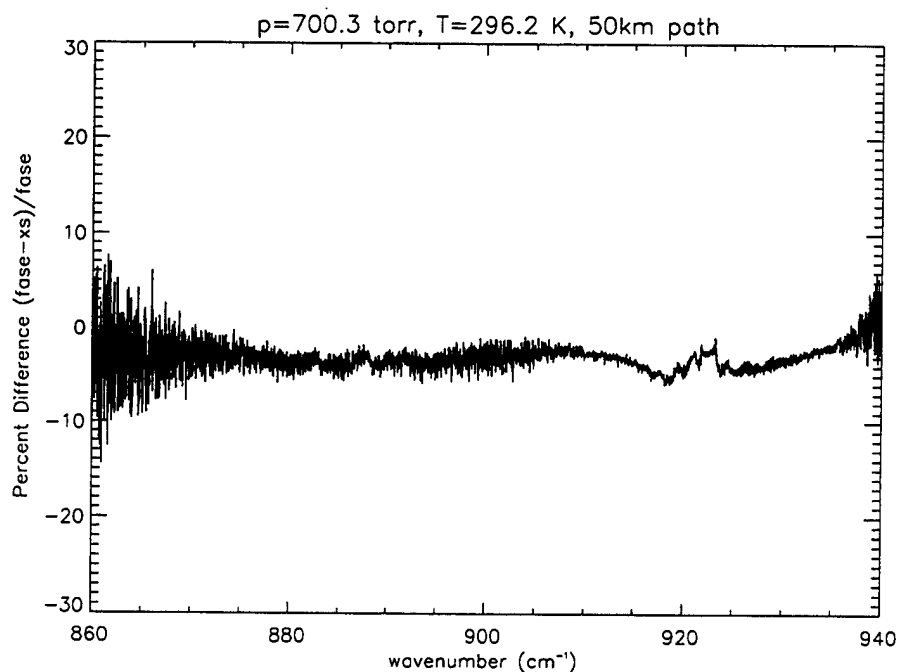


Figure 12 Percent Difference Between the Cross-Section Computed with Pseudo-Lines and the Data from Varanasi for a 50km Path at $p=700.3$ torr, $T=296.2$ K

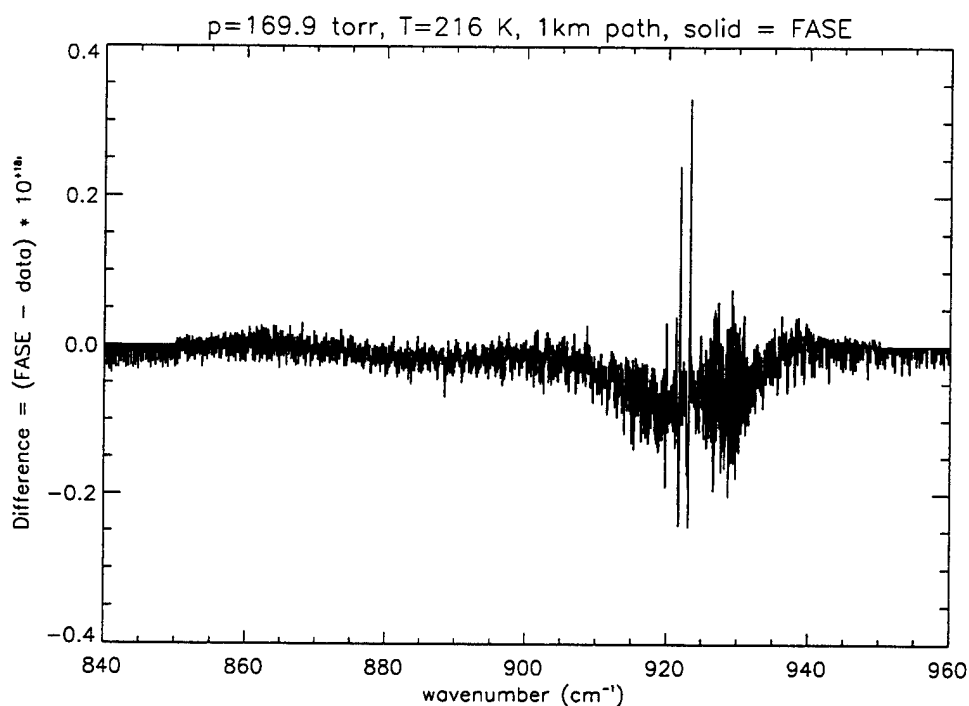


Figure 13 Difference Between Computed and Measured Cross-Section for a 1km Path at $p=169.9$ torr, $T=216.0$ K

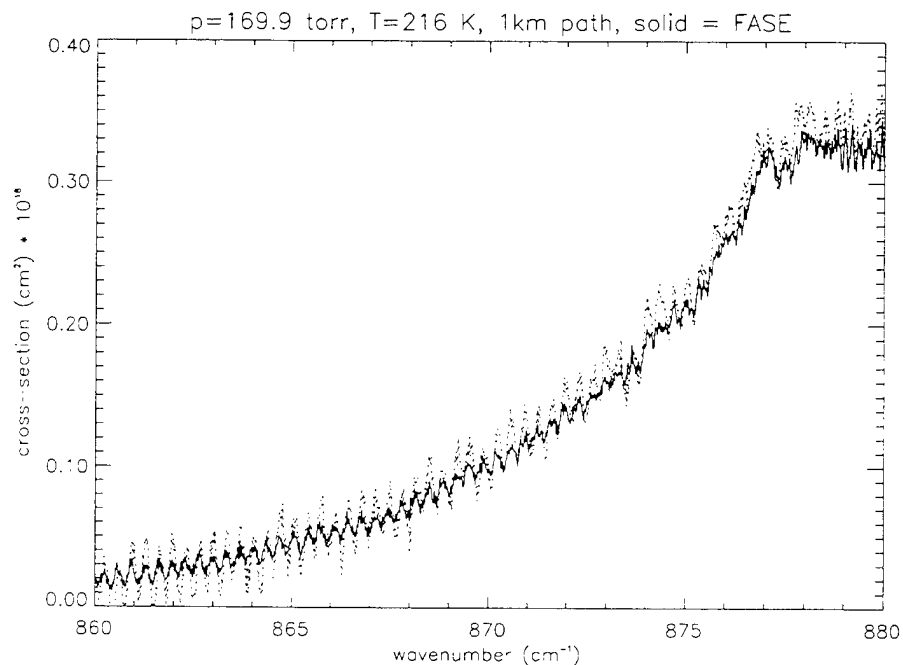


Figure 14 Comparison of the Computed Cross-Section (Solid Line) with the Measured Cross-Section (Dotted) for the Conditions Given in Figure 7 Over the Range 860-880 cm^{-1}

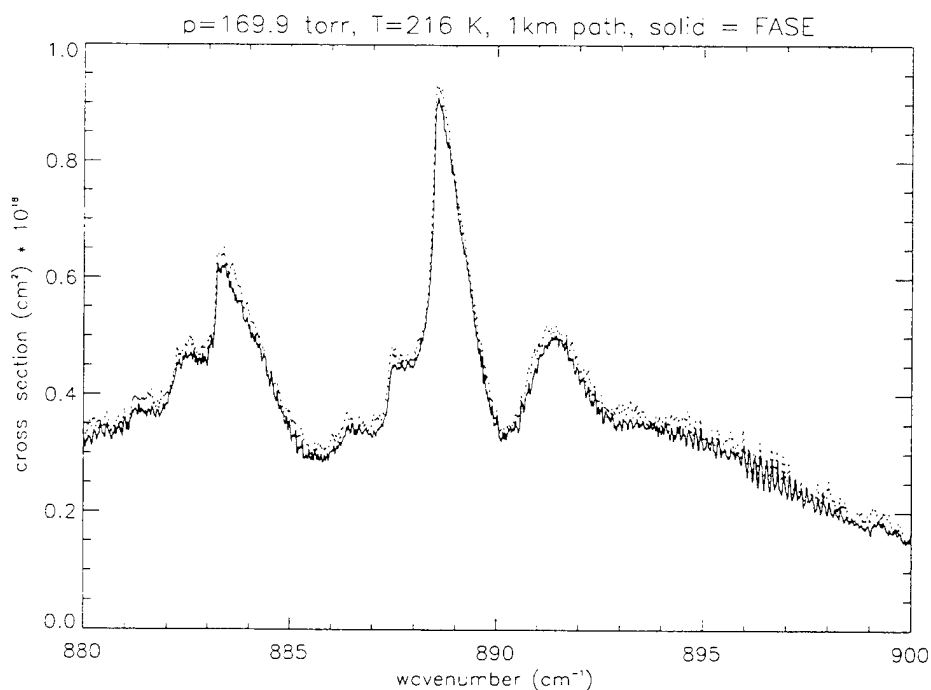


Figure 15 Comparison of the Computed Cross-Section (Solid Line) with the Measured Cross-Section (Dotted) for the Conditions Given in Figure 7 Over the Range 880-900 cm^{-1}

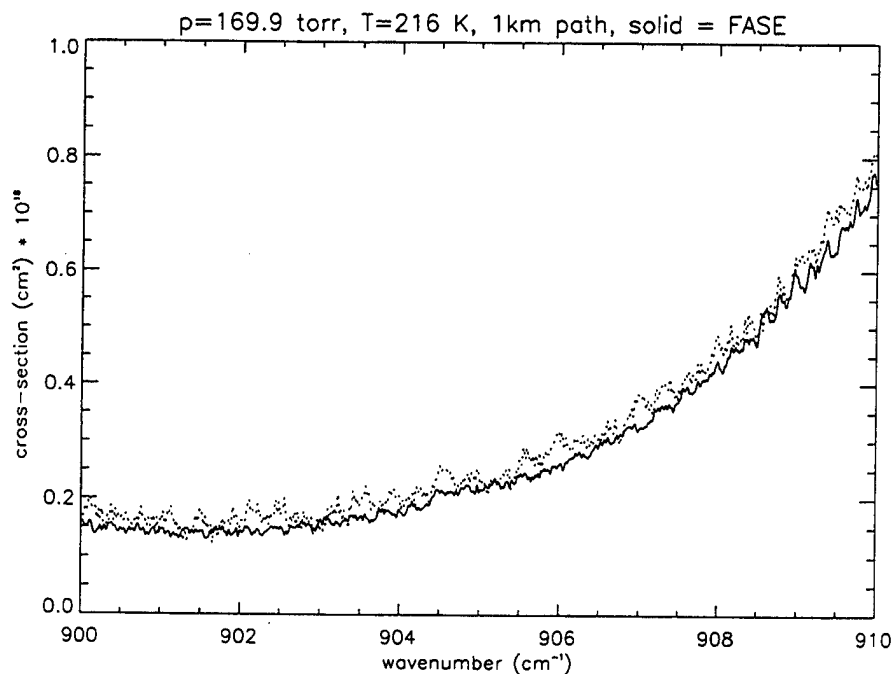


Figure 16 Comparison of the Computed Cross-Section (Solid Line) with the Measured Cross-Section (Dotted) for the Conditions Given in Figure 7 Over the Range 900-910 cm^{-1}

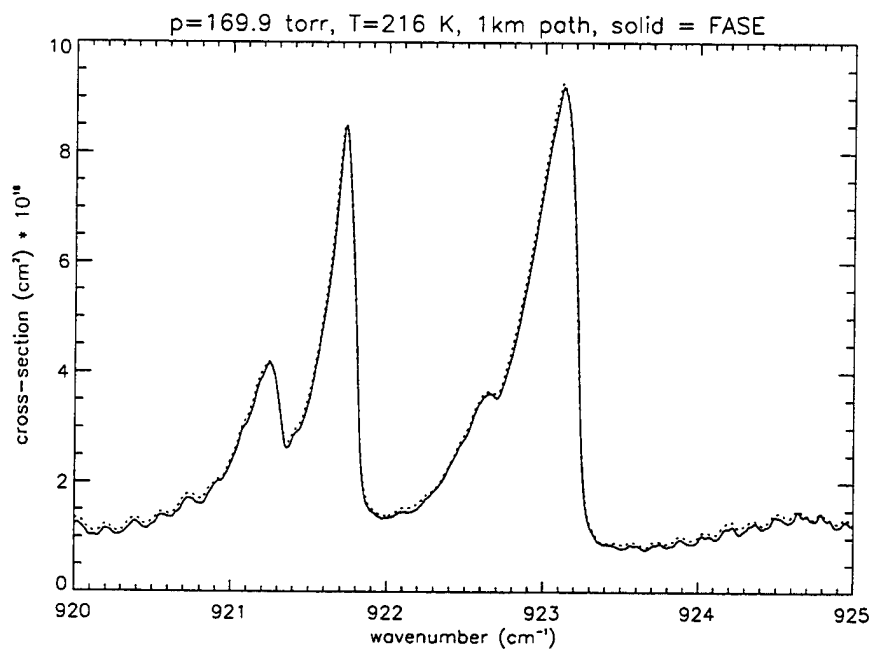


Figure 17 Comparison of the Computed Cross-Section (Solid Line) with the Measured Cross-Section (Dotted) for the Conditions Given in Figure 7 Over the Range 920-925 cm^{-1}

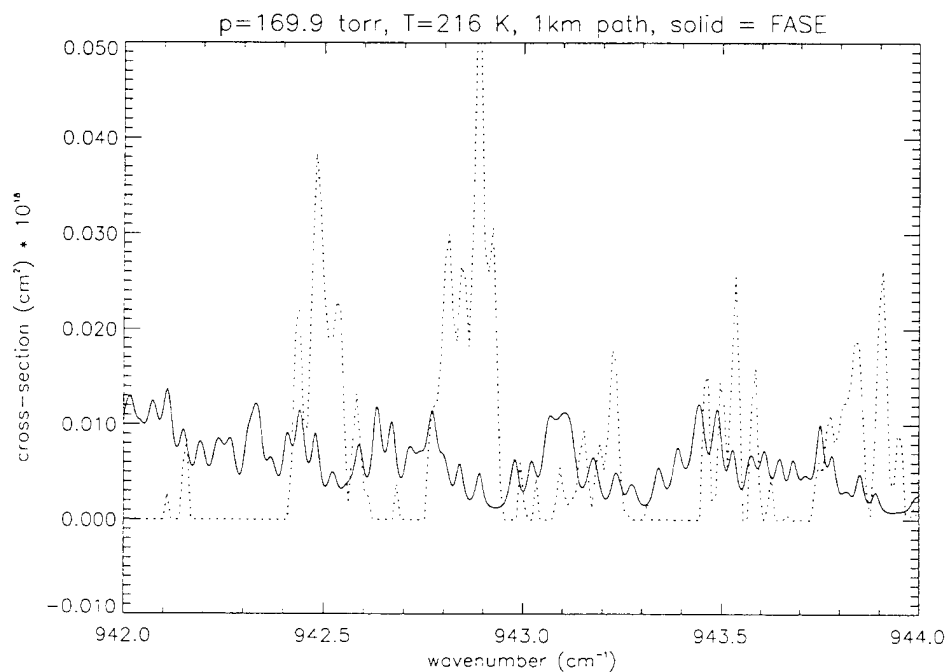


Figure 18 Comparison of the Computed Cross-Section (Solid Line) with the Measured Cross-Section (Dotted) for the Conditions Given in Figure 7 Over the Range 942-944 cm^{-1}

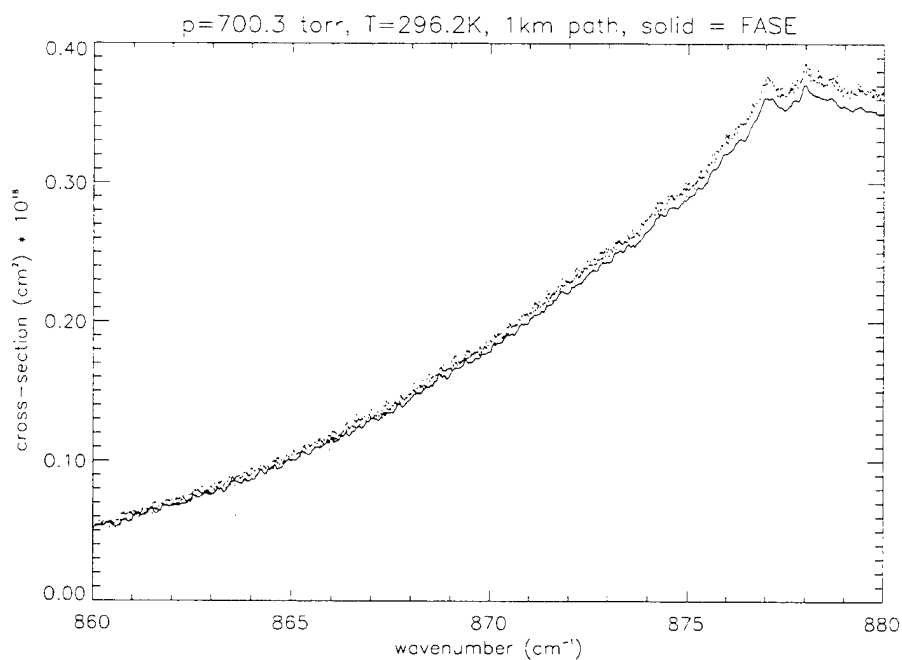


Figure 19 Comparison of the Computed Cross-Section (Solid Line) with the Measured Cross-Section (Dotted) for the Conditions Given in Figure 8 Over the Range 860-880 cm^{-1}

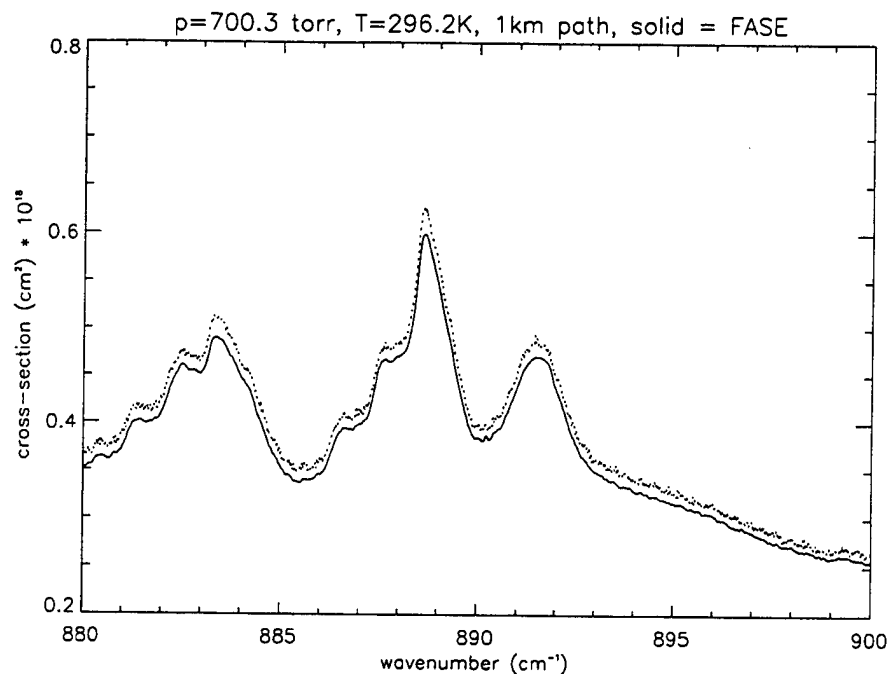


Figure 20 Comparison of the Computed Cross-Section (Solid Line) with the Measured Cross-Section (Dotted) for the Conditions Given in Figure 8 Over the Range 880-900 cm^{-1}

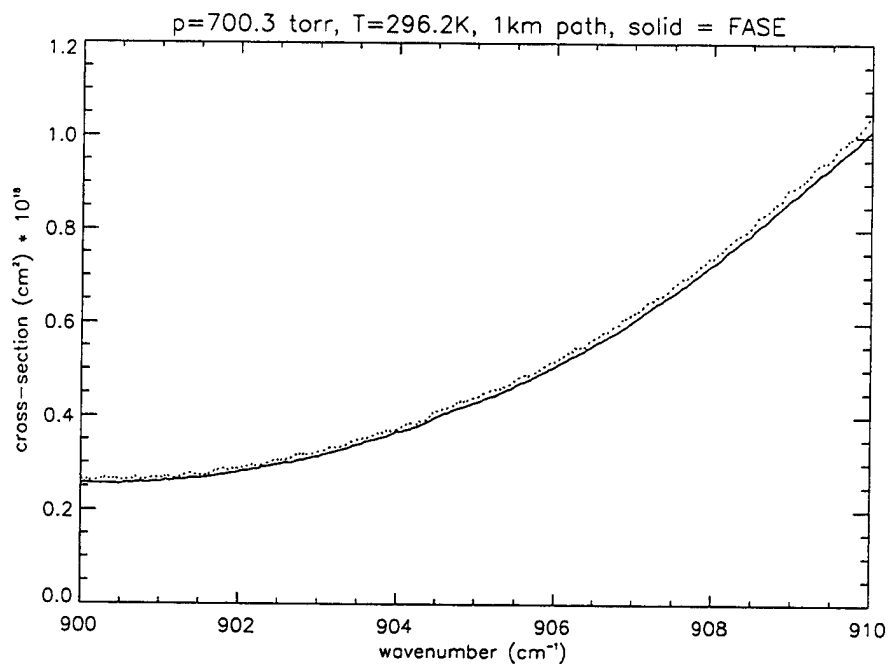


Figure 21 Comparison of the Computed Cross-Section (Solid Line) with the Measured Cross-Section (Dotted) for the Conditions Given in Figure 8 Over the Range 900-910 cm^{-1}

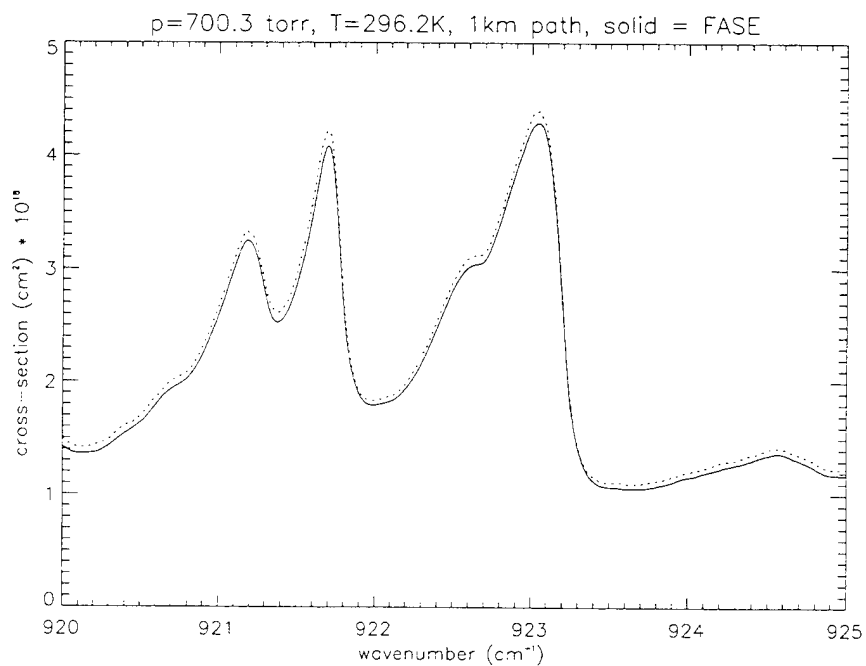


Figure 22 Comparison of the Computed Cross-Section (Solid Line) with the Measured Cross-Section (Dotted Line) for the Conditions Given in Figure 8 Over the Range 920-925 cm^{-1}

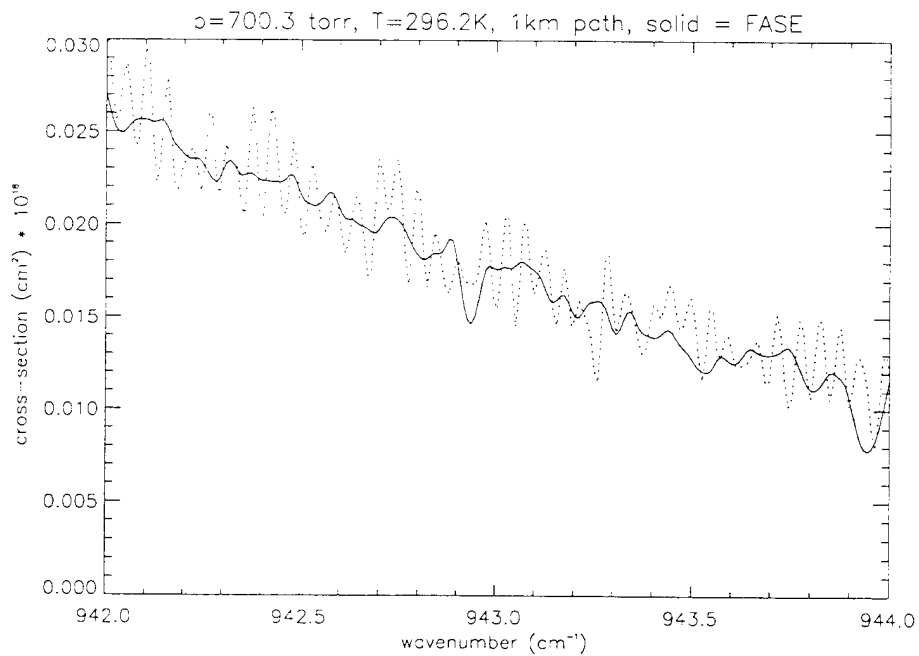


Figure 23 Comparison of the Computed Cross-Section (Solid Line) with the Measured Cross-Section (Dotted) for the Conditions Given in Figure 8 Over the Range 942-944 cm^{-1}

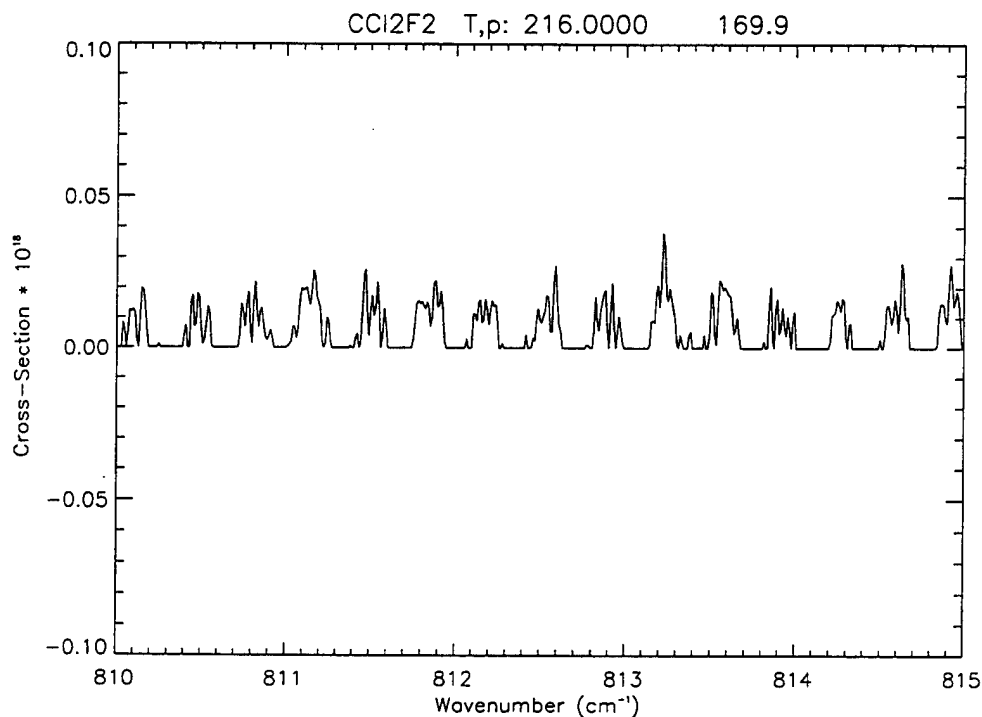


Figure 24 Measurements of F-12 in the Far Wings of the Band

In general, there is a slight offset between the calculated cross-sections and the Varanasi data for the 169.9 torr, 216.0 K case (Figure 14 through Figure 18). The peak-to-peak magnitude of the features in Figure 14 is somewhat less for the calculated cross-sections than for the data. In Figure 15 the peak-to-peak values are better, but there is some difference in the shape of the calculation. This is evident around 887, 893, and 895-896 cm^{-1} . The differences in shape are especially noticeable in Figure 16, from 900 - 910 cm^{-1} , which has the worst agreement for this case (except for the wing regions where the absorption is very weak). The region around the band center is plotted in Figure 17 and one can see that there is a slight offset, but otherwise very good agreement between the computation and the data. Finally, Figure 18 shows a region in the wings of the band where there appears to be much more noise than real data.

The comparisons of the measured data with calculations using the pseudo-lines for 770.3 torr and 296.2 K are given in Figure 19 through Figure 23. These figures show a much more distinct offset than Figure 14 through Figure 18. While the structure is difficult to determine in Figure 18, it appears to match the data very well (especially from 877 - 878 cm^{-1}). The peak-to-peak agreement is also very good in Figure 19 and Figure 21, while Figure 20 clearly shows the offset. As with Figure 18, Figure 23 gives an indication that the agreement in the wings of the band is very poor.

The above comparisons lead to another aspect of the problem that must be evaluated, namely the determination of meaningful values for the cross-section and the establishment of a frequency cutoff for the inclusion of pseudo-lines in the calculation. What is necessary is a reasonable criterion for determining a wavenumber cutoff whereby the noise in the data coupled with uncertainties in the calculation combine to make it impossible to determine the validity of the cross-section. What will be important is a combination of the small magnitude of the cross-section in this cutoff region and the magnitude of overlapping contributions of other species (which may completely mask the weak absorption of the cross-section). A means of understanding the errors in the cross section computed using the pseudo-lines and in the Varanasi data can be obtained through a propagation of errors analysis.

As described above, the absorption coefficient computed by FASE is the optical thickness divided by the path absorber amount. Thus the error in the absorption coefficient can be expressed as the sum of the individual errors:

$$\Delta k_{\text{calc}} \cong \Delta \tau \left(\frac{\partial k_{\text{calc}}}{\partial \tau} \right) + \Delta N \left(\frac{\partial k_{\text{calc}}}{\partial N} \right) \quad \text{Eq. 20}$$

which reduces to

$$\Delta k_{\text{calc}} \cong \frac{1}{N} (\Delta \tau - \Delta N k_{\text{calc}}) \quad \text{Eq. 21}$$

For the calculations shown above, the appropriate values for Eq. 21 are given in Table 14. These values yield an uncertainty in the absorption coefficient of about 1% for $k=1.0\text{e-}17$ (center of band), and an uncertainty approaching 10% in the wings of the band.

The errors for the measured data can be determined in two ways. First, a qualitative examination of the measurements in the wings of the band shows a random variation of about 0.1%. A somewhat more quantitative method is to use the reported error bars (Varanasi and Nemtchinov, 1994) for the variation in the integrated cross-section: $\Delta S=0.07\text{e-}17$, where S is the integral of k over the entire band:

$$S = \int \frac{k_{\text{meas}}(\sigma) d\sigma}{N_0} \approx \sum \frac{k_{\text{meas}}(\sigma) \Delta \sigma}{N_0} \quad \text{Eq. 22}$$

and N_0 is used to convert the units of k ($\text{cm}^{-1} \text{ atm}^{-1}$) to the given units of S (cm molecule^{-1}). Note that the units are slightly different from the ones used in earlier equations, but they conform to the reported values. If one assumes that ΔS and N_0 are known, the variation in S can be

attributed to the variations in k . Assuming that the variations in k are random throughout the band, the error in k can be written as:

$$\Delta k_{\text{meas}}(\sigma) = \frac{\Delta S(\sigma) N_0}{\sum \Delta \sigma} \quad \text{Eq. 23}$$

where the denominator represents the entire bandwidth. Using the values in Table 14, the error in the absorption coefficient is less than 0.2%, which is similar to that determined by examination of the measurement. In this table, N is the path absorber amount (molecules cm^{-2}) and the 1% error is attributed to how this number is written to the output files; τ is the optical thickness and its error is the stated numeric error of FASE; k is the absorption cross-section (cm^2), ΔS is the error in the integrated cross-section (cm molecule^{-1}) (from Varanasi and Nemtchinov, 1994); N_0 is Loschmidt's number ($\text{molecule cm}^{-3} \text{ atm}^{-1}$); and $\Delta \sigma$ is the spectral band width (cm^{-1}). Because of the weak signal in the wings of the band, and because the assumption that the error in the integrated cross-section can be attributed to the absorption coefficient equally throughout the band, it is not clear if either of these error values are appropriate when examined individually. However, their consistency would indicate that 0.1-0.2% represents a reasonable guess.

Table 14 Values Used in Propagation of Error Calculations

Quantity	Value (order of magnitude)
N	$1.0\text{e}+14$
ΔN	$1\% = 1.0\text{e}+12$
τ	$1.0\text{e}-03$
$\Delta \tau$	$0.5\% = 5.0\text{e}-06$
k	$1.0\text{e}-17$
ΔS	$0.013\text{e}-17$
N_0	$2.687\text{e}+19$
$\Delta \sigma$	100

4.5.2. Pseudo-Line Timing Tests

The ability to read the new cross-section data as a series of pseudo-lines is an inexpensive alternative to developing a more sophisticated interpolation/extrapolation scheme. However, the price paid is one of algorithm timing. The inclusion of pseudo-lines can add anywhere from thousands to tens of thousands of spectral lines to a given calculation. For calculations, which

require a large number of atmospheric layers, this can add a significant amount of time to the calculation.

A series of tests was conducted in the spectral range from 725 - 1245 cm^{-1} using the heavy molecule species F-11, F-12, and CCl_4 . These species were chosen because they have data in the form of 'old' cross-sections and 'new' pseudo-lines. Calculations were done for the uplooking radiance and transmittance from 0 - 40 km and 0 - 100 km with a US Standard Atmosphere. The timing results given in Table 15 represent an average of eight individual runs for each case, and the standard deviation for each case was less than 3 seconds.

The calculations from 100 km to the surface take longer than those from 40 km because of an increased number of atmospheric layers, and because the upper layers require higher spectral resolution than the lower layers. With the cross-sections, calculations from 100 km take approximately 3.1 times longer than those from 40 km. The difference is larger with the pseudo-lines, a factor of about 3.5, because each pseudo-line must be accurately computed at each layer. In reality, the concentration profiles of many species, the heavy molecules in particular, decrease rapidly with altitude. Using the option to zero the contribution from weak lines when they no longer contribute significantly to the overall optical depth (NOZERO=0 on input RECORD 3.1) dramatically decreases the computation time for both the pseudo-line and cross-section cases. For the 0-100 km case shown here there is a 20% timing penalty for using the pseudo-lines instead of the cross-sections, which is small compared to the change in accuracy with this new data.

Table 15 Timing Test Results

Case	Old Cross-Section	New Pseudo-Line
0 - 40	178.96	401.11
0 - 100	562.93	1413.07
0 - 100 (zero small absorber amounts)	263.02	327.36

4.5.3. Pseudo-Line Algorithm Implementation

4.5.3.1. Line File Creation (LNFL)

A minimal amount of changes were required to LNFL (the program used to select line parameters from the HITRAN database and put them in the correct format for FASCODE and LBLRTM) in order to accommodate the pseudo-lines. The lines are read from an 'external data

tape' and merged with the lines from HITRAN. There are 36 molecules in the current version of HITRAN and the pseudo-lines were given IDs starting with 51. Consequently, the dimensions of arrays, the parameters "NTMOL" and "NSPECI", and read/write format statements needed to be changed to accommodate the additional molecules. Data statements relating to the molecule name, the number of isotopes (1) and the isotope ID number (assumed to be 111) were also changed, and the temperature dependence of the halfwidth was set at 0.5 (Toon, 1995).

4.5.3.2. Main Program and Subroutines

In all of the files listed below, the parameter statements "NTMOL" (the total number of molecules allowed) and "NSPECI" (the total number of isotopes allowed) were changed from 36 and 79 to 64 and 90. These parameters are used to define array sizes in dimension statements; additional species will require further changes to "NSPECI", but not "NTMOL" (until the total number of molecules is greater than 50).

fasatm.f

The name of the molecules ('HMOLEC') and the corresponding molecular weights ('AIRMWT') were set appropriately. The molecular weight was set to 1.0 for each of the pseudo-line species so that the Doppler width will be essentially the same as the grid spacing and the pseudo-lines can never become too strong (Toon, 1995).

fase01.f / nonlte.f

The only changes are to the parameter statements listed above.

oprop.f

In addition to the parameter statements listed above and molecular weight ("SMASSI") and isotope information ("ISONM" and "ISO82"), the changes to this file involve the partition functions and degeneracy factors. The inputs required for calculating the partition sums were provided by Toon (1995). The formulas for the vibrational partition function (Q_v), the stimulated emission term (S_e), and the rotational partition function (Q_r) are given as:

$$Q_v = \prod \left[1 - \exp \left(- \frac{h c \nu_j}{k T} \right) \right]$$

$$S_e = 1 - \exp \left(- \frac{h c \nu_i}{k T} \right)$$

$$Q_r = \left(\frac{296}{T} \right)^b$$
Eq. 24

with $b = 1.5$, the fundamental vibrational frequencies, ν_j , listed in Table 16, and ν_i the center frequency of the line in question.

Table 16 Fundamental Vibrational Frequencies for F-12

ν_j (cm^{-1})
1102
667
468
262
321
1161
462
923
437

4.5.4. Execution of FASE with Pseudo-Lines

Atmospheric input to FASE is accomplished through the use of the module "FASATM". "FASATM" is used to select the atmospheric profile to be used by the module and sets up the layers. "FASATM" is set from the "IATM" parameter, contained in RECORD 1.2. When "IATM" is set to 1, FASE is instructed to look to RECORD 3 for specification of the atmospheric profile. Input parameters for "FASATM" are located in RECORDS 3.1 through 3.6 of the TAPE5 input file.

The number of molecular species desired is set from RECORD 3.1 with the "NMOL" parameter. "NMOL" must be set to be at least equal to the highest number of the molecule desired. Molecules from the HITRAN Database have been given molecule identification numbers 1-36 while pseudo-lines are given molecule identification numbers 51-60. Some of the

HITRAN 96 and pseudo-line molecules do not have internally stored profiles (see Table 17) and for these species the user must explicitly specify the atmosphere.

FASE employs a user-defined atmospheric profile when the parameter "MODEL" is set to 0 (zero) in RECORD 3.1. RECORDs 3.4 through 3.6 contain the information required for a user-defined atmospheric profile. Contained within RECORD 3.4, "IMMAX" is the number of atmospheric profile boundaries to be read in by the model. RECORD 3.5 contains the physical parameters required to define a boundary.

Table 17 Molecules Without Profiles

HITRAN-96		Pseudo-Lines	
ID Number	Molecule	ID Number	Molecule
29	COF ₂	52	CF ₄
30	SF ₆	57	F-142b
31	H ₂ S	60	SF ₆
32	HCOOH		
33	HO ₂		
34	O-Atom		

Note that if one wishes to run with the first seven molecules and pseudo-lines, one can specify a profile for molecules 1-7 and the pseudo-line, and zero for the remainder of the species. Also note that FASE does not check to see if more than one of the same species has been selected. For example, CLONO₂ has lines, pseudo-lines, and cross-sections.

4.6. Cloud/Rain Upgrades

Changes to the cloud and rain routines have been employed based on improvements that have been developed for MODTRAN (Berk, 1995). This set of upgrades makes it easier to modify the cloud/rain models (by re-configuring and clarifying the coding structure) as well as providing for a more flexible prescription of realistic cloud and aerosol layers and their associated optical properties. The improved layering scheme allows for multiple overlapping and non-overlapping clouds. For cumulus and stratus type clouds, with and without rain, the upgrades include:

- adjustable cloud parameters (thickness, altitude, vertical extinction, water/ice column amounts, humidity, and scattering phase functions),
- decoupling of the clouds from aerosols (allowing clouds and aerosols to be present at the same altitude),

- the introduction of ice particles, and
- a flexible set of user-defined cloud spectral properties, and water droplet, ice particle, and rain rate profiles.

Cloud profiles are merged with other atmospheric profiles by combining and adding layer boundaries where necessary. The cloud profiles will be merged with existing layers if the cloud layer boundary is within 0.5m of an atmospheric boundary level, otherwise a new atmospheric boundary level is created. (The number of available levels is controlled by the parameter "LAYDIM"). The cloud/rain profiles used by the code are written to TAPE6.

Figure 25 illustrates calculations with the new cloud models. The cloud consisted of a cumulus cloud with overlying cirrus (the cloud top and cirrus thickness were held constant) and the figure shows the change in radiance with a change in cloud thickness and base height. The marked change in radiance for a cloud with a base at 0.4 km and one at 1.88 km shows the need for a versatile cloud simulation capability, even for direct radiance and transmittance (no scattering) calculations.

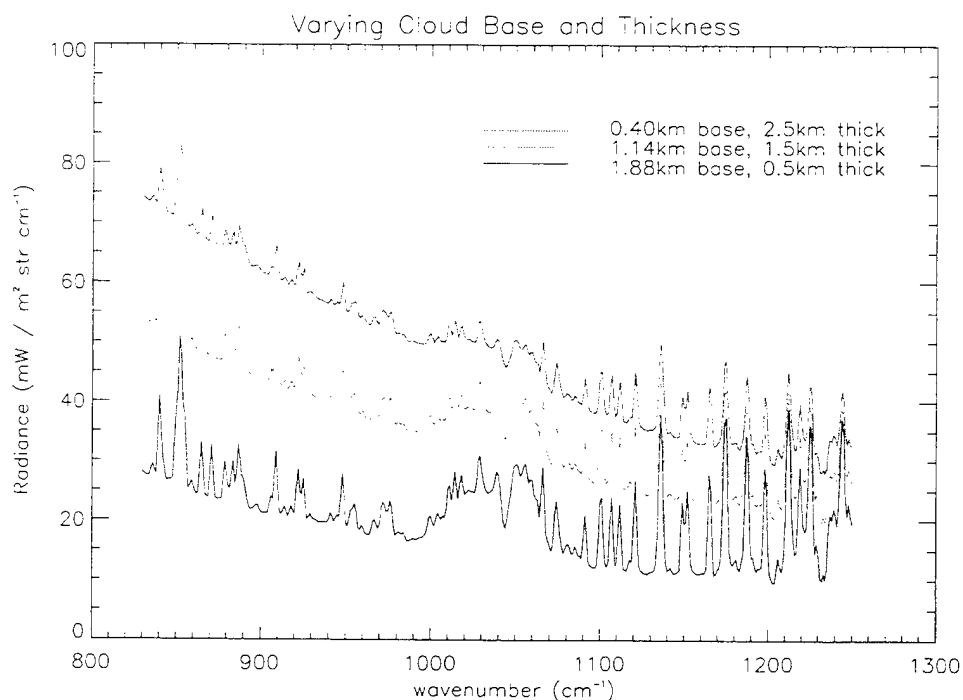


Figure 25 Example of the New FASE Cloud Options: User has the Ability to Change Cloud Base Altitude and Thickness

5. Suggestions for Future Upgrades and Model Validation

There are several areas of development in which FASE is still incomplete. Of these, the most significant is the absence of a capability for including multiple scattering. In addition, there are a number of validations that should be performed in order to confirm the continued accuracy of the model. The following section discusses suggested areas for future development.

5.1. Multiple Scattering

Multiple scattering was eliminated from the development of LBLRTM. For FASE it was decided that it was not cost-effective to re-implement the 2-stream multiple scattering routines that had been a part of FASCODE. While FASE does have the option to create the output files that can be used as input to multiple scattering codes, a coherent interface between FASE and one such code should be pursued. The likely candidate for coupling with FASE is the multiple scattering model CHARTS. The advantage to this code (over the other major code, DISORT) is that it is designed to work with the panel structure of LBLRTM, rather than the monochromatic input required for DISORT. That is, the amount of calculation overhead is reduced when running CHARTS over a broad spectral region, making it uniquely suited for coupling with FASE.

5.2. Cloud/Rain Upgrades

There are now further upgrades to the cloud and rain routines available from MODTRAN4. To maintain consistency in the common elements of the Air Force radiance and transmittance codes, these upgrades should be added to FASE.

5.3. Beta-Test Results

FASE has not been released to the general public, but rather to a limited set of users ('beta-testers') who were encouraged to report problems with the code and suggest new features or enhancements to the existing code. While most of the problems have been fixed, a few issues remain, mainly related to the new cloud and aerosol routines. Beta-test users of FASE at the Air Force Research Laboratory-Hanscom have identified problems in the new cloud/aerosol routines when doing calculations in the microwave. Investigation of the cause of these problems led to the identification of several errors in the implementation of the upgrades from MODTRAN. Fixing these errors did not solve the microwave problems, and this work should continue.

5.4. Calibration and Validation

An important part of the acceptance of FASCODE/FASE over other publicly available radiative transfer models is the on-going calibration and validation. Examples of this include participation in the ICRCCM testing and the validation of the model with ARM data .

6. Summary

Significant progress has been made in the merging of FASCODE and LBLRTM to create FASE. The result is a radiative transfer model that contains state-of-the-art atmospheric physics through validations of LBLRTM with ARM data, while also incorporating many of the features from FASCODE which are not found in LBLRTM but are required for flexible use of the codes under airborne, ground- and space-based conditions. Future updates to FASE should include a coupling of the code to multiple-scattering routines. Further, FASE should continue to undergo comparisons with other models and validation against measurements from the DOE ARM site as well as a variety of DoD datasets.

7. References

- Acharya, P.K., D.C. Robertson, and A. Berk, *Upgraded Line-of-Sight Geometry Package and Band Model Parameters for MODTRAN*, PL-TR-93-2127, Phillips Laboratory Directorate of Geophysics, Hanscom AFB, Massachusetts, May 1993. ADA280952.
- Anderson, G. P., F.X. Kneizys, E.P. Shettle, L.W. Abreu, J.H. Chetwynd, R. E. Huffman, and L. A. Hall, UV Spectral Simulations Using LOWTRAN7, in Advisory Group for Aerospace Research and Development (AGARD) Conference Proc. 454, 1990.
- Anderson, G. P., et al., History of One Family of Atmospheric Radiative Transfer Codes, The European Symposium on Satellite Remote Sensing, Conference on Passive Infrared Remote Sensing of Clouds and Atmosphere II, 26-30 September 1994, Rome, Italy.
- Anderson, G. P., et al., 1995, *FASCODE/MODTRAN/LOWTRAN: Past/Present Future*, Proceedings of the 18th Annual Review Conference on Atmospheric Transmission Models, 6-8 June, 1995, Phillips Lab/Geophysics Directorate, Hanscom AFB.
- Anderson, G. P., Phillips Laboratory Directorate of Geophysics, Private Communication, 1994.
- Berk, A., Upgrades to the MODTRAN Layer Cloud/Rain Models, *Rpt. No. SSI-SR-56*, Spectral Sciences, Inc., 99 S. Bedford St., Burlington, MA, 01803, 1995.
- Chetwynd, J.H., Phillips Laboratory Directorate of Geophysics, Private Communication, 1994.
- Clough, S.A. and F.X. Kneizys, Convolution Algorithm for the Lorentz Function, *Applied Optics*, 18, 2329, 1979.
- Clough, S.A., F.X. Kneizys, L. S. Rothman, and W.O. Gallery, Atmospheric spectral transmittance and radiance: FASCODE1B, SPIE V.277, Atmospheric Transmission, 1981.
- Clough, S.A., et al., Radiative Transfer Model Development in Support of the Atmospheric Radiation Measurement (ARM) Program, Proceedings of the Second ARM Science Team Meeting, DOE Conf. 9303112, Norman, OK, 1-4 March 1993.
- Clough, S.A. and P. Brown, Atmospheric and Environmental Research, Inc, Private Communication, 1994.
- Edlen, K., The Refractive Index of Air, *Metrologia*, 2, 12, 1966.
- Gallery, W.O., F.X. Kneizys, and S.A. Clough, *Air Mass Computer Program for Atmospheric Transmittance/Radiance Calculations: FSCATM*, AFGL-TR-83-0065, Air Force Geophysics Laboratory, Hanscom AFB, Massachusetts, (NTIS AD A 132108), 1983.

- Gallery, W.O. and S.A. Clough, *FFTSCAN: A Program for Spectral Smoothing Using Fourier Transforms*, PL-TR-92-2131, Geophysics Directorate/Phillips Lab, Hanscom AFB, Massachusetts, 1992.
- Hall, L.A. , and G. P. Anderson, High-Resolution Solar Spectrum between 2000 and 3100 Å, *J. Geophys. Res.*, **96**, 12927-12931, 1991.
- Isaacs, R.G. W.-C. Wang, R. D. Worsham and S. Goldenberg, Multiple Scattering LOWTRAN and FASCODE Models, *Applied Optics*, **26**, 1272-1281, 1987.
- Li, Z., and P. Varanasi, Measurement of the Absorption Cross-Section of CFC-11 at Conditions Representing Various Model Atmospheres, *J. Quant. Spectrosc. Radiat. Transfer*, **52**, 137-144, 1994.
- Kneizys, F.X., E.P. Shettle, W.O. Gallery, J.H. Chetwynd, Jr., L.W. Abreu, J.E.A. Selby, R.W. Fenn, and R.A. McClatchey, *Atmospheric Transmittance/Radiance: Computer Code LOWTRAN 5*, AFGL-TR-80-0067, Air Force Geophysics Laboratory, Hanscom AFB, Massachusetts, 21 February 1980. ADA088215.
- Kneizys, F.X., E.P. Shettle, W.O. Gallery, J.H. Chetwynd, Jr., L.W. Abreu, J.E.A. Selby, S.A. Clough, and R.W. Fenn, *Atmospheric Transmittance/Radiance: Computer Code LOWTRAN 6*, AFGL-TR-83-0187, Air Force Geophysics Laboratory, Hanscom AFB, Massachusetts, 1 August 1983. ADA137689.
- Kurucz, R.L., The Solar Irradiance by Computation, in Proc. of the 17th Annual Review Conference on Atmospheric Transmission Models, 7 June 1994, Geophysics Directorate/Phillips Laboratory, Hanscom AFB, MA, 1994.
- Miller, S.M., H. E. Snell, and J.-L. Moncet, Simultaneous Retrieval of Middle Atmospheric Temperature and Trace Gas Species Volume Mixing Ratios from CIRRIS, *J. Geophys. Res.*, **104**, 18,697-18,714, 1999.
- Minschwaner, K., G. P. Anderson, L. A. Hall, and K. Yoshino, Polynomial Coefficients for Calculating O₂ Schumann-Runge Cross Sections at 0.5 cm⁻¹ Resolution, *J. Geophys. Res.*, **97**, 10103-10108, 20 June 1992.
- Minschwaner, K., G. P. Anderson, L. A. Hall, R. J. Thomas, D. Rusch, A. Berk, and J. Conant, Scattered Ultraviolet Radiation in the Upper Stratosphere 3: Modeling and Analysis, *J. Geophys. Res.*, in press 1995.
- Moncet, J.-L., and S.A. Clough, CHARTS: Code for high resolution accelerated radiative transfer with scattering, in *IRS '92: Current Problems in Atmospheric Radiation*, Keevallik and Karner, editors, A. Deepak, pp. 493-494, 1992.
- Ridgway, W.L., R.A., Moose, and A. C. Cogley, *Atmospheric Transmittance/Radiance Computer Code FASCOD2*, Air Force Geophysics Laboratory Technical Report AFGL-TR-82-0392, 1982. ADA130241.
- Rothman, L. S., et al., The HITRAN Molecular Database: Editions of 1991 and 1992, *J.Q.S.R.T.*, **48**, 469-507, 1992.

- Rothman, L. S., and A. McCann, *HITRAN96*, Phillips Laboratory Geophysics Directorate, Hanscom AFB, Massachusetts, released on CD-ROM, 1996.
- Shettle, E.P., and S.M. Anderson, Ozone Cross-Sections for the Chappuis and Wulf Absorption Bands, private communication from G.P. Anderson, 1995.
- Smith, H.J.P., D. J. Dube, M.E. Gardner, S.A. Clough, F.X. Kneizys, and L. S. Rothman, *FASCODE: Fast Atmospheric Signature Code (Spectral Transmittance and Radiance)*, AFGL-TR-78-0081, Air Force Geophysics Laboratory, Hanscom AFB, Massachusetts 1978. ADA057506.
- Stamnes, K., S.C. Tsay, W.J. Wiscombe, and K. Jayaweerra, Numerically Stable Algorithm for Discrete-Ordinate-Method Radiative Transfer in Multiple Scattering and Emitting Layered Media, *Appl. Opt.*, 27, 2502-2509, 1988.
- Toon, G., Jet Propulsion Laboratory, Private Communication, November - December 1995.
- Varanasi, P., and V. Nemtchinov, Thermal Infrared Absorption Coefficients of CFC-12 at Atmospheric Conditions, *J. Quant. Spectrosc. Radiat. Transfer*, 51, 679-687, 1994.
- Wang, J., Phillips Laboratory Directorate of Geophysics, Private Communication, 1994.

Appendix A: Spectral Grid Algorithm

In FASCODE, the spectral grid is optimized individually for each layer. Layer spectral quantities (optical depth, transmittance or radiance) are combined by interpolating the coarser grid onto the finer grid. The layer dv is set by default to one fourth the average Voigt halfwidth for that layer. This value represents a compromise between adequately sampling the spectrum and minimizing the number of spectral points. For example, for the US Standard Atmosphere, the dv varies between about 0.03 cm^{-1} at the ground and about 0.0003 cm^{-1} at 30 km.

At the time FASCODE was first designed, computer memory and disk space were limited and minimizing the number of spectral points was critical. However, the cost of keeping a separate dv for each layer is the need for repeated spectral interpolation when combining layers. Using the same dv for all layers would eliminate the need for spectral interpolation, a viable alternative since the increased requirements for memory and disk space are not constraining factors on current computer systems.

This system of using the same spectral grid spacing for all layers was implemented in the model XFWD, a modified version of FASCODE developed internally at AER (Miller et al., 1999). Both models calculate the optical depth at a spectral resolution appropriate for the layer. XFWD then interpolates these values to the final resolution before computing the radiative transfer. In contrast, FASCODE computes the radiative transfer by interpolating the results from the previous layer onto the grid of the current layer and merging the results. The result of this merge is written to a "scratch" file. This procedure is repeated from the lowest altitude layer (largest dv) to the highest (smallest dv). In XFWD all of the optical depth calculations are completed before the radiative transfer is done, and all calculations are carried out in memory. The difference in doing the radiative transfer on a fixed wavenumber grid can be seen by comparing the times to compute the optical depth and the radiative transfer.

Timing comparisons were conducted between FASCODE and XFWD in order to see how the proposed program structure and the output of optical depths at the same spectral resolution for each layer would change the CPU time. The timing tests were conducted for calculations over the spectral region $1010 - 1130 \text{ cm}^{-1}$. To eliminate subtle differences in the methods of computing molecular amounts, the same atmosphere was input to both models (11 layers for the limb-viewing case, 15 layers for the up- and down-looking cases, all with U.S. Standard Atmosphere conditions) and the same line file was used (first 12 species from the HITRAN database). The continuum was not implemented, but in both cases it is only a minor contributor

to the total computation time. The cases tested are representative of the type of calculations for which FASCODE is used. The fact that not all of the features were implemented should not impact the timing results; while only a single comparison is discussed for each case, the results agree with numerous other runs of the two models. Table A- 1 provides the total CPU time required for both models when each of the test cases was run. The models were both found to use the same percentage of CPU time relative to actual time, indicating that system usage did not contribute to timing differences. Both models were run on a "SPARCcenter 1000" computer. These times are shown for each of the test case conditions in Table A- 2, Table A- 3, and Table A- 4.

Table A- 1 Model Comparisons for Total CPU Run Time

CASE	FASCOD3P (seconds)	XFWD(seconds)
12 km tangent height	275.53	188.33
0 km - 100 km (up-looking)	309.22	186.12
100 km - 0 km (down-looking)	317.03	215.21

Table A- 2 Case1: Limb Calculation with 12km Tangent Height

LAYER	FASCOD3P		XFWD	
	Optical Depth	Radiative Transfer	Optical Depth	Radiative Transfer
1	2.70	0.98	4.05	3.61
2	3.76	1.70	4.40	3.52
3	6.92	3.38	5.83	3.49
4	10.28	5.58	8.70	3.55
5	21.47	10.57	14.08	3.54
6	21.21	11.71	17.05	3.44
7	20.99	11.62	17.80	3.49
8	21.08	11.64	18.43	3.51
9	20.90	11.54	19.22	3.58
10	24.98	13.62	19.48	3.58
11	25.19	13.72	20.14	3.85
Total	179.48	96.06	149.18	39.16
Percentage	65%	35%	79%	21%

Table A- 3 Case 2: Looking Up: 0km - 100km

LAYER	FASCOD3P		XFWD	
	Optical Depth	Radiative Transfer	Optical Depth	Radiative Transfer
1	1.96	0.26	3.60	1.99
2	1.75	0.34	2.34	1.94
3	1.90	0.43	2.36	1.86
4	2.19	0.68	2.48	1.88
5	3.06	1.24	2.93	1.97
6	5.23	2.42	4.33	1.94
7	7.64	3.74	5.70	1.94
8	11.01	5.92	8.74	1.95
9	16.30	8.44	13.93	1.85
10	25.35	13.11	16.87	1.83
11	25.12	13.83	17.65	1.83
12	25.25	14.43	18.22	1.76
13	25.40	13.92	19.17	1.79
14	24.87	13.83	19.59	1.78
15	25.63	14.02	19.88	1.98
Total	202.66	106.61	157.79	28.29
Percentage	65%	35%	85%	15%

Table A- 4 Case 3: Looking Down: 100km - 0km

LAYER	FASCOD3P		XFWD	
	Optical Depth	Radiative Transfer	Optical Depth	Radiative Transfer
1	2.15	0.28	4.15	2.16
2	1.87	0.35	4.06	2.12
3	2.08	0.45	4.21	2.00
4	2.27	0.67	4.25	2.06
5	3.22	1.26	4.74	2.00
6	5.47	2.60	6.21	1.99
7	7.74	3.79	7.69	1.93
8	11.43	5.78	10.86	1.89
9	16.79	8.69	15.97	1.81
10	25.91	13.31	19.04	1.78
11	25.51	15.30	20.08	1.70
12	25.64	14.16	18.52	1.65
13	25.38	14.26	21.34	1.62
14	26.49	14.25	21.90	1.58
15	25.87	14.07	24.12	1.81
Total	207.82	109.22	187.14	28.10
Percentage	66%	34%	87%	13%

The timing for the optical depth calculations is similar in FASCODE and XFWD because they are calculated at the same monochromatic spectral resolution ($\Delta\nu$) in each program. Minor differences in the timing occur because the optical depths are interpolated to the final $\Delta\nu$ in XFWD while they are output to disk in FASCODE. However, what is important to note is that for a particular calculation the radiative transfer time is a constant for XFWD while it increases in FASCODE as the $\Delta\nu$ decreases. The FASCODE timing for radiative transfer listed in the above tables includes I/O time while in the case of XFWD there is no I/O. Looking at Case 1, in Table A- 2, we can assume that since the $\Delta\nu$'s for the two models are the same for Layer 11, the time to compute the radiative transfer should also be the same. This implies that 9.87 seconds in FASCODE (out of a total of 13.72 seconds) can be attributed to the I/Os. Thus it is clear that a significant fraction of the radiative transfer computation time in FASCODE consists of I/O, especially at lower pressures.

From these timing results we may make the following conclusions:

- (1) The I/Os are a limiting factor and make up more than 80% of the total FASCODE radiative transfer time in up- and down-looking cases.
- (2) I/Os are suppressed in XFWD by making optimal use of the available core memory. However, the radiative transfer time in XFWD is affected by the fact that the calculations are done at high spectral resolution. We estimate that this feature accounts for an increase of about 100% in the radiative transfer time over that of FASCODE (not including FASCODE I/O). Nonetheless radiative transfer represents only a small fraction (13-21%) of the total computation time, which indicates that the impact of this structure on the total time is minimal (7-10%).

One should also note that the dv is pre-set by the user in XFWD. In the case where the atmosphere is truncated at, for example, Layer 2, the optical depth would be interpolated to a dv appropriate for Layer 2 and not the high dv of Layer 15 as in the above examples. In general, dv should never be set smaller than the smallest dv in the layering scheme.

Comparisons of FASCODE and LBLRTM timing using a "benchmark" input developed for LBLRTM were conducted on a (non-vectorized) "SPARCcenter 1000" computer. Tests were also done to compare timing differences resulting from changes to the Voigt lineshape algorithm. These tests indicated that changes in the Voigt algorithm resulted in an increase of about 10% in the LBLRTM computation time. This increase was subsequently reduced to about 7% through the efficient re-coding of some sections of the algorithm. Improvements in the structure of the LBLRTM read and write routines ("BUFIN" and "BUFOUT") should also favorably impact the timing on non-vectorized machines. In general, the total CPU time for LBLRTM (after the Voigt changes) is about a factor of two less than that for an identical FASCODE calculation. These improvements in the code to reduce the computation time are included in FASE.